



THE UNIVERSITY *of* EDINBURGH

Edinburgh Research Explorer

Functional brain defects in a mouse model of a chromosomal t(1;11) translocation that disrupts DISC1 and confers increased risk of psychiatric illness

Citation for published version:

Bonneau, M, O'Sullivan, ST, Gonzalez-Lozano, MA, Baxter, P, Gautier, P, Marchisella, E, Hardingham, NR, Chesters, RA, Singh, Y, Didier, M, Koopmans, F, Semple, CA, McIntosh, AM, Volkmer, H, Loos, M, Fox, K, Hardingham, G, Vernon, AC, Porteous, DJ, Smit, AB, Price, D & Millar, JK 2021, 'Functional brain defects in a mouse model of a chromosomal t(1;11) translocation that disrupts DISC1 and confers increased risk of psychiatric illness', *Translational Psychiatry*. <https://doi.org/10.1038/s41398-021-01256-3>

Digital Object Identifier (DOI):

<https://doi.org/10.1038/s41398-021-01256-3>

Link:

[Link to publication record in Edinburgh Research Explorer](#)

Document Version:

Peer reviewed version

Published In:

Translational Psychiatry

General rights

Copyright for the publications made accessible via the Edinburgh Research Explorer is retained by the author(s) and / or other copyright owners and it is a condition of accessing these publications that users recognise and abide by the legal requirements associated with these rights.

Take down policy

The University of Edinburgh has made every reasonable effort to ensure that Edinburgh Research Explorer content complies with UK legislation. If you believe that the public display of this file breaches copyright please contact openaccess@ed.ac.uk providing details, and we will remove access to the work immediately and investigate your claim.



1 **Functional brain defects in a mouse model of a chromosomal t(1;11) translocation**
2 **that disrupts *DISCI* and confers increased risk of psychiatric illness**

3

4 Marion Bonneau¹, Shane T. O'Sullivan¹, Miguel A. Gonzalez-Lozano², Paul Baxter³,
5 Phillippe Gautier⁴, Elena Marchisella⁵, Neil R. Hardingham⁶, Robert A. Chesters⁷, Helen
6 Torrance¹, David M. Howard^{8,9}, Maurits A. Jansen¹⁰, Melanie McMillan¹¹, Yasmin Singh¹²,
7 Michel Didier¹³, Frank Koopmans², Colin A. Semple⁴, Andrew M. McIntosh⁹, Hansjürgen
8 Volkmer¹⁴, Maarten Loos⁵, Kevin Fox⁶, Giles E. Hardingham³, Anthony C. Vernon^{7,15}, David
9 J. Porteous¹, August B. Smit², David J. Price³, J. Kirsty Millar^{1*}

10

11 ¹Centre for Genomic and Experimental Medicine, MRC Institute of Genetics and Molecular
12 Medicine at the University of Edinburgh, Edinburgh, UK

13 ²Department of Molecular and Cellular Neurobiology, Center for Neurogenomics and
14 Cognitive Research, VU University, Amsterdam, The Netherlands

15 ³Centre for Discovery Brain Sciences, Hugh Robson Building, The University of Edinburgh,
16 Edinburgh, UK

17 ⁴MRC Human Genetics Unit, MRC Institute of Genetics and Molecular Medicine at the
18 University of Edinburgh, Edinburgh, UK

19 ⁵Sylics Synaptologics BV, Amsterdam, The Netherlands

20 ⁶School of Biosciences, Museum Avenue, Cardiff University, Cardiff, UK

21 ⁷Department of Basic and Clinical Neuroscience, Institute of Psychiatry, Psychology and
22 Neuroscience, King's College London, London, UK

23 ⁸Social, Genetic and Developmental Psychiatry Centre, Institute of Psychiatry, Psychology &
24 Neuroscience, King's College London, UK

25 ⁹Division of Psychiatry, Kennedy Tower, The University of Edinburgh, Edinburgh, UK

26 ¹⁰Edinburgh Preclinical Imaging, The Chancellor's Building, The University of Edinburgh,
27 Edinburgh, UK,

28 ¹¹Centre for Reproductive Health, The Queen's Medical Research Institute, The University of
29 Edinburgh, Edinburgh, UK

30 ¹²Centre for Genomics and Transcriptomics, Paul-Ehrlich-Straße 23, Tübingen, Germany

31 ¹³Translational Sciences at Sanofi, Chilly-Mazarin, France

32 ¹⁴Department of Molecular Biology, NMI Natural and Medical Sciences Institute at the
33 University of Tübingen, Reutlingen, Germany

34 ¹⁵MRC Centre for Neurodevelopmental Disorders, King's College London, London, UK

35

36 *Corresponding author

37 Tel: +44 (0)131 651 8732

38 Fax: +44 (0)131 651 1059

39 Email: kirsty.millar@igmm.ed.ac.uk

40 Address: Centre for Genomic and Experimental Medicine, MRC Institute of Genetics and
41 Molecular Medicine at the University of Edinburgh, Crewe Road, Edinburgh, EH4 2XU, UK

42

43 Running title: t(1;11) mouse model

44

45 **Abstract**

46 A balanced t(1;11) translocation that directly disrupts *DISC1* is linked to schizophrenia and
47 affective disorders. We previously showed that a mutant mouse, named *Der1*, recapitulates
48 the effect of the translocation upon *DISC1* expression. Here, RNAseq analysis of *Der1*
49 mouse brain tissue found enrichment for dysregulation of the same genes and molecular
50 pathways as in neuron cultures generated previously from human t(1;11) translocation
51 carriers via the induced pluripotent stem cell route. *DISC1* disruption therefore apparently
52 accounts for a substantial proportion of the effects of the t(1;11) translocation. RNAseq and
53 pathway analysis of the mutant mouse predict multiple *Der1*-induced alterations converging
54 upon synapse function and plasticity. Synaptosome proteomics confirmed that the *Der1*
55 mutation impacts synapse composition, and electrophysiology found reduced AMPA:NMDA
56 ratio in hippocampal neurons, indicating changed excitatory signalling. Moreover,
57 hippocampal Parvalbumin-positive interneuron density is increased, suggesting that the
58 *Der1* mutation affects inhibitory control of neuronal circuits. These phenotypes predict that
59 neurotransmission is impacted at many levels by *DISC1* disruption in human t(1;11)
60 translocation carriers. Notably, genes implicated in schizophrenia, depression and bipolar
61 disorder by large-scale genetic studies are enriched among the *Der1*-dysregulated genes,
62 just as we previously observed for the t(1;11) translocation carrier-derived neurons.
63 Furthermore, RNAseq analysis predicts that the *Der1* mutation primarily targets a subset of
64 cell types, pyramidal neurons and interneurons, previously shown to be vulnerable to the
65 effects of common schizophrenia-associated genetic variants. In conclusion, *DISC1*
66 disruption by the t(1;11) translocation may contribute to the psychiatric disorders of
67 translocation carriers through commonly affected pathways and processes in
68 neurotransmission.

69

70 **Introduction**

71 Psychiatric illnesses such as schizophrenia and recurrent affective disorders have a
72 substantial underlying genetic component. Considerable progress has been made in recent
73 years towards identification of the multitude of genes involved using large-scale studies of
74 genome-wide association (GWAS) and recurrent copy number variants (CNVs)¹⁻⁶. GWAS
75 tends to identify genomic loci with common, but small, individual effects that encompass
76 several genes, leaving the specific causal genes unidentified, unless further refinements are
77 applied. In contrast, recurrent CNVs are rare, tending to exert a strong effect (most likely due
78 to large changes in expression levels of the genes at fault), but also usually encompass
79 multiple genes. Chromosomal rearrangements, such as translocations, linked to psychiatric
80 disorders are rarer still, but can have the advantage of strong effects and accurate
81 pinpointing of genes due to their disruption by the breakpoints of the rearranged genomic
82 segments. It is likely that convergence of data arising from genomic events such as these
83 will assist in revealing the genes and mechanisms that predispose to major mental illness.

84 One example of a chromosomal rearrangement linked to psychiatric disorders is a
85 t(1;11) translocation that substantially increases risk of developing schizophrenia or affective
86 disorders in a large Scottish family⁷⁻⁹. The psychiatric symptoms presented by t(1;11)
87 translocation carriers are typical, that is, they are within the range of current diagnostic
88 criteria, and are accompanied by reduced white matter integrity¹⁰, cortical thickness¹¹ and
89 prefrontal cortex gyrification⁹, all typical of schizophrenia. Carriers of the t(1;11) translocation
90 also have decreased glutamate levels in the dorsolateral prefrontal cortex⁹. Moreover,
91 transcriptome analysis of induced pluripotent stem cell (iPSC)-derived cortical neurons from
92 t(1;11) translocation carriers¹² found enrichment for dysregulated genes at putative
93 schizophrenia and depression loci discovered through large scale GWAS and CNV studies<sup>1-
94 3</sup>, potentially identifying some of the genes of interest at those loci, and indicating that the
95 t(1;11) translocation may trigger disease pathways shared with schizophrenic patients who
96 are not translocation carriers.

97 The t(1;11) translocation directly disrupts the *DISC1* gene on chromosome 1¹³.
98 *DISC1* encodes a potential molecular scaffold protein involved in multiple critical functions in
99 the developing and adult brain^{14, 15}, including neurogenesis¹⁶⁻¹⁸, neuronal cargo trafficking¹⁹⁻²³
100 and neurotransmission²³⁻²⁶. *DISC1* disruption is therefore likely to contribute substantially to
101 mechanisms leading to psychiatric illness in t(1;11) translocation carriers.

102 Two apparently non-coding genes of unknown function, *DISC2* and *DISC1FP1*
103 (otherwise known as *Boymaw*), are also disrupted on chromosomes 1 and 11, respectively¹³,
104 ²⁷, and potential genetic modifier loci have been identified within the family²⁸, all of which
105 may additionally impact disease mechanisms in t(1;11) translocation carriers. It is now
106 important to discover how each of these disruptions and putative modifiers relate to the gene
107 expression changes, brain structure alterations and psychiatric symptoms of t(1;11)
108 translocation carriers.

109 To examine the impact of *DISC1* disruption in isolation from the additional
110 complexities of *DISC2* disruption and loss of normal *DISC1FP1* function, and of potential
111 genetic modifiers, we have utilised a mutant mouse which accurately recapitulates the
112 effects of the translocation upon *DISC1* expression¹². IPSC-derived neural precursor cells
113 and cortical neurons from t(1;11) translocation carriers exhibit reduced *DISC1* expression¹².
114 Chimeric transcripts encoding aberrant C-terminally truncated chimeric forms of *DISC1* are
115 also produced in the IPSC-derived neural cells as a result of fusion between the *DISC1* and
116 *DISC1FP1* genes on the derived chromosome 1^{12, 29}. The mutant mouse was precisely
117 engineered to mimic the fusion between *DISC1* and *DISC1FP1* on the derived 1
118 chromosome and exhibits reduced *Disc1* levels plus chimeric transcript expression¹². This
119 mutant mouse is referred to as *Der1*.

120 Heterozygous *Der1* mice express reduced levels of wild-type *Disc1* plus the aberrant
121 chimeric transcripts^{12, 29}. Because *Disc1* multimerises³⁰, there is thus potential in
122 heterozygotes for dominant-negative effects due to interaction between wild-type and mutant
123 *Disc1*. Homozygotes, however, lack any wild-type *Disc1* and may express high levels of
124 aberrant *Disc1*. Despite heterozygotes corresponding most closely to t(1;11) translocation

125 carriers, we opted to study both mutant genotypes in order to obtain the most complete
126 understanding of the likely effects of DISC1 disruption. A flow chart (Supplementary Figure
127 1) illustrates the experimental approach taken, with the aim of allowing the results described
128 here to be compared with previously published t(1:11) translocation studies and integrated
129 with psychiatric genetic association studies of single nucleotide polymorphism (SNP) and
130 CNV variants in the general population. We combine magnetic resonance imaging (MRI),
131 histology, transcriptomics, synaptosome proteomics and electrophysiology to demonstrate
132 that the *Der1* mutation primarily affects cellular properties rather than brain structure, and
133 that it targets a variety of cell types including neurons. Patterns of gene expression and
134 predictions of altered biological processes substantially overlap between *Der1* cortex and
135 IPSC-derived cortical neuron cultures from t(1:11) translocation carriers. We find widespread
136 dysregulation of genes implicated as potential common risk factors for schizophrenia,
137 depression and bipolar disorder. We therefore propose that *DISC1* disruption targets
138 common pathways shared with psychiatric patients who do not carry the t(1:11)
139 translocation, to contribute to the elevated risk of major mental illness displayed by t(1:11)
140 translocation carriers⁹.

141

142 **Materials and methods**

143 Detailed materials and methods are provided in the Supplementary information file.

144

145 **Results**

146 **Adult *Der1* mutant mice show no overt changes in brain structure**

147 Using ex vivo structural MRI, we found no evidence for effects of the *Der1* mutation on
148 overall brain volume or the volumes of 51 brain regions analysed individually
149 (Supplementary Table 1). In the absence of hypotheses arising from the MRI analysis of
150 brain structure, and given that DISC1 is highly expressed in the hippocampus from early
151 development through to adulthood, and that prefrontal cortex (PFC) is affected in t(1:11)
152 translocation carriers⁹, these regions were explored in further detail. The *Der1* mutation does

153 not affect cell densities in the hippocampal Stratum, Radiatum, Lacunosum and Moleculare
154 or prefrontal cortex, nor the thickness of individual cortical layers within the barrel cortex, nor
155 the total cortical thickness in either the barrel cortex or the PFC (Supplementary Figure 2, 3,
156 4).

157

158 **RNAseq analysis of adult *Der1* cortex and hippocampus**

159 We next conducted RNASeq using wild-type and heterozygous 'cortex' (consisting of
160 cortices minus hippocampus, cerebellum and olfactory bulbs) and hippocampus. The
161 resulting data were analysed at the whole gene and single exon levels using DESeq2³¹ and
162 DEXSeq³², respectively. Full-length *Disc1* expression is reduced in heterozygous *Der1*
163 mouse whole brain as detected by quantitative RT-PCR and immunoblotting¹². RNAseq also
164 found reduced *Disc1* expression in heterozygous *Der1* cortex and hippocampus (Figure 1a,
165 Supplementary Table 2a, c), confirming the validity of these datasets.

166 Expression of 30,121 genes was detected in cortex, of which 2,124 and 3,568 are
167 differentially expressed in heterozygotes at the whole gene or exon level respectively (all
168 corrected $p < 0.05$, Figure 1b, Supplementary Table 2a, b). Expression of 28,049 genes was
169 detected in hippocampus, of which 175 and 52 are differentially expressed in heterozygotes
170 at the whole gene or exon level respectively (all adjusted $p < 0.05$, Supplementary Table 2c,
171 d).

172

173 **Expression Weighted Cell-type Enrichment (EWCE) analysis of RNASeq data** 174 **suggests specific cell types are targeted by the *Der1* mutation**

175 EWCE analysis³³ was used to look for evidence that certain cell types are especially
176 vulnerable to the *Der1* mutation. We utilised gene expression profiles generated by
177 hierarchical clustering of single cell RNASeq profiles from 9,970 mouse brain cells and
178 around 15,000 of the most abundantly expressed genes, resulting in 24 cell classes, referred
179 to as the KI Superset³⁴. The authors of that study calculated 'specificity values' for each
180 gene within each cell class, to indicate enrichment for expression of that gene in a cell class

181 compared to the other classes in the Superset³⁴. EWCE analysis was used here to
182 determine whether there is enrichment for *Der1*-induced dysregulation of genes with high
183 specificity values for Superset cell classes in cortex (Figure 1c). Statistical significance was
184 observed for pyramidal neurons ('pyramidal somatosensory', 'pyramidal CA1' [which also
185 encompasses neurons from CA2 and the subiculum³⁴]), interneurons ('cortical interneuron',
186 'striatal interneuron'), dopaminergic neurons ('dopaminergic adult neurons', 'hypothalamic
187 dopaminergic neurons'), 'oxytocin/vasopressin-expressing neurons' and
188 'astrocytes/ependymocytes'. *Der1* hippocampus dysregulated genes are also highly
189 enriched in several cell classes (Figure 1d). Of these, pyramidal neurons ('pyramidal
190 somatosensory'), 'medium spiny neuron' and 'interneuron' achieved statistical significance.
191 'Pyramidal CA1' reached initial significance in *Der1* hippocampus, but did not survive
192 multiple testing correction. Pyramidal CA1, pyramidal somatosensory and medium spiny
193 neurons should reside primarily in the hippocampus, cortex and striatum, respectively, thus
194 some of these findings were initially unexpected. However, the previously published
195 hierarchical clustering of cell classes³⁴ indicated that 'pyramidal CA1' and 'pyramidal
196 somatosensory' are highly similar, with medium spiny neurons the next most closely related
197 cell type. We therefore infer that in cortex and hippocampus the *Der1* mutation may target
198 general features shared between these three neuron classes.

199 Based on these findings, Parvalbumin-expressing interneuron density was quantified
200 in adult PFC and hippocampus. PFC shows no change (Supplementary Figure 5), however
201 there is a trend towards an increase in the dentate gyrus ($p=0.07$), and a significant increase
202 in *Der1* heterozygotes when the whole hippocampus is examined (34% increase, Figure 1e,
203 f). The EWCE analysis data pointing to hippocampal interneuron targeting could therefore be
204 due, at least partially, to increased density of interneurons expressing Parvalbumin at high
205 levels. This contrasts with previous reports of reduced Parvalbumin-positive cell density in
206 mice expressing mutant DISC1, or in response to endogenous Disc1 knockdown³⁵.

207 We also hypothesised that the cell types most affected by the *Der1* mutation might
208 be susceptible to apoptosis, as quantified using Activated-Caspase-3. Of the adult PFC and

209 hippocampal regions examined, there is a trend towards increased apoptosis in CA1
210 ($p=0.06$, Supplementary Figure 6), which may indicate that CA1 cells are particularly
211 vulnerable. This could lead to reduced cell density in CA1, a parameter that unfortunately
212 could not be adequately examined due to the prohibitively tight packing of cells in this region.

213

214 **RNASeq deconvolution suggests that cell class proportions are unaltered by the *Der1*** 215 **mutation**

216 RNASeq deconvolution was carried out utilising gene expression data (rather than the
217 specificity values used above for EWCE analysis) for the most highly enriched genes from
218 the 24 cell classes of the Superset³⁴. First, the ability of the deconvolution programme,
219 CIBERSORT³⁶, to deconvolve the 24 cell classes was examined by generating artificial *in*
220 *silico* samples with varying proportions of each cell class (Supplementary Figure 7). Using
221 two specificity value thresholds, CIBERSORT was able to deconvolve most cell types. The
222 exceptions include embryonic cell types, which should be absent from our *Der1* samples,
223 and rarer cell types in adult brain such as neural progenitors and neuroblasts. When used to
224 deconvolve *Der1* cortex and hippocampus whole gene DESeq2 RNASeq data, CIBERSORT
225 found no evidence for an effect of the mutation upon the relative proportion of any of the cell
226 classes examined (Supplementary Figure 8). The increased density of hippocampal
227 Parvalbumin-positive interneurons (Figure 1e, f) therefore may not represent a general effect
228 upon all hippocampal interneuron types. Likewise, the trend towards increased hippocampal
229 CA1 apoptosis (Supplementary Figure 6) does not translate to a detectably decreased
230 density of pyramidal CA1 neurons, possibly because this Superset class also contains
231 pyramidal neurons from CA2 and the subiculum³⁴.

232

233 **Molecular pathway analysis predicts wide-ranging effects of the *Der1* mutation**

234 Since the patterns of gene dysregulation are not explained by overtly altered cell
235 proportions, the RNASeq data were next used to predict effects upon canonical pathways.
236 Ingenuity Pathway Analysis (IPA), an unbiased method for examining transcriptomic data

237 using statistical significance and magnitude plus direction of fold-change, was carried out
238 using the whole gene level DESeq2 data, or combined DESeq2 plus exon level DEXSeq
239 data. This analysis predicts effects upon diverse pathways including metabolic, stress-
240 response and important neurosignalling processes (Figure 2a). A selection of these
241 pathways, based on statistical significance or relevance to later parts of this study, are
242 discussed below.

243 Mitochondrial dysfunction, including increased oxidative phosphorylation is strongly
244 predicted, based largely upon upregulated whole gene expression of multiple complex I, III
245 and IV components (Supplementary Figure 9), consistent with DISC1's known role in
246 regulating oxidative phosphorylation^{37, 38}. Moreover, the chimeric transcripts expressed by
247 *Der1* mice encode aberrant mitochondrial species that induce mitochondrial dysfunction²⁹.

248 Also upregulated at the whole gene level is the mitochondrial pathway 'Fatty acid β -
249 oxidation I' (Supplementary Figure 10) which degrades fatty acids to release energy.
250 Dysregulated enzymes feeding into this pathway are involved in fatty acid synthesis and
251 break down. Together these changes imply altered levels of lipids, which are critical for
252 many brain processes.

253 The 'CREB signalling in neurons' pathway (Figure 2b) is activated by cell surface
254 glutamate receptors, including AMPA and NMDA receptors, and calcium channels. It
255 regulates gene expression changes that are critical for synaptic plasticity and long-term
256 potentiation (LTP), both known to be DISC1-modulated³⁰. DISC1 is also already known to
257 regulate CREB signalling³⁰, and in our study IPA predicts that downregulation of *Creb1*
258 activity is responsible for many of the gene expression changes ($p=9e-9$, $z=-3$). Indeed,
259 there is enrichment (hypergeometric $p=0.02$) for dysregulation of genes containing
260 conserved cAMP-Response Elements (CREs, <http://natural.salk.edu/creb/>, Supplementary
261 Table 3) in heterozygous *Der1* cortex, with 203 (9.6%) of the genes dysregulated at the
262 whole gene level having CREs. The *Der1* mutation potentially affects activation of the
263 pathway via AMPA receptor subunit degradation³⁹, and NMDA receptor membrane
264 dynamics and surface expression¹². Moreover, genes encoding glutamate receptors,

265 including AMPA and NMDA receptor subunits, and several synaptic scaffolds are
266 dysregulated (Figure 2b).

267 Using the combined dysregulated DESeq2 plus DEXSeq data, IPA also determined
268 that many cellular functions are enriched for differentially expressed genes (Table 1,
269 Supplementary Table 4a). Predictions relating to neurotransmission, synaptic plasticity and
270 LTP are related to the 'CREB signalling in neurons' pathway above, plus genes encoding
271 inhibitory signalling factors, such as subunits of GABA_A and GABA_B receptors. Predictions
272 relating to vesicle transport and exo/endocytosis are based on dysregulated genes encoding
273 vesicle trafficking factors; voltage-gated calcium channel subunits as well as synaptotagmins
274 and syntaxins that together mediate calcium-dependent neurotransmitter release;
275 components of the exocyst complex; and components of the endocytic Clathrin-associated-
276 Adaptor-Protein-Complex. The wide-ranging neuronal morphology and cytoskeleton-related
277 predictions are based on multiple genes involved in diverse relevant processes. Similarly,
278 the cell-cell contact/adhesion-related functions are widespread, but notably encompass
279 genes required for early synapse formation, such as latrophilins, as well as maintenance of
280 trans-synaptic connections, for example neuroligins and neuroligins. Other predictions relate
281 to cell proliferation, neuronal migration and circadian rhythms. All of these processes are
282 already known to involve DISC1^{12, 16, 18, 21, 25, 35, 40-43}.

283 *Der1* hippocampus RNASeq data were similarly analysed. IPA did not strongly
284 predict any canonical pathway changes due to the relatively small number of changes, but
285 did predict altered functions that largely reflect those for cortex (Supplementary Table 4b, 5),
286 and there is enrichment for dysregulation of 86 shared genes (39% of the total dysregulated
287 hippocampal genes, Supplementary Table 2c, d) in both regions ($p=7e-11$). Myelination is
288 also predicted to be affected, consistent with previous studies demonstrating DISC1
289 involvement in oligodendrocyte differentiation and function⁴⁴⁻⁴⁶.

290 Numerous processes are thus predicted to be affected by the *Der1* mutation in cortex
291 and hippocampus, with striking convergence upon neurotransmission.

292

293 **Molecular pathway analysis of targeted cell types identified by EWCE analysis**

294 EWCE analysis identified cell classes that may be targeted by the *Der1* mutation (Figure 1c,
295 d). We reasoned that the cell class-enriched gene expression changes may inform on the
296 impact of the *Der1* mutation in each cell type. Pathway analysis was therefore carried out
297 using the cell class-enriched dysregulated genes (Supplementary Table 6, 4c). *Der1* cortex
298 pyramidal neuron (CA1 and somatosensory) and interneuron terms relate to synaptic
299 transmission. *Der1* cortex astrocyte/ependymocyte terms relate to lipid metabolism and
300 uptake of glutamine/glutamate. The lipid metabolism predictions are based on upregulation
301 of genes encoding enzymes involved in fatty acid β -oxidation, and other aspects of brain
302 lipid metabolism. This is related to the *Der1* cortex RNASeq canonical pathway prediction
303 'Fatty Acid β -oxidation I' (Figure 2a), and indicates a potential imbalance between lipid
304 synthesis and oxidation. Since astrocytes are a major source of brain lipid which is widely
305 utilised, including for synapse function⁴⁷ and myelination by oligodendrocytes⁴⁸, these
306 processes may be compromised via astrocyte dysfunction. The glutamine/glutamate uptake
307 predictions are based on dysregulated expression of genes such as *Slc1a2*, which encodes
308 the synaptic glutamate transporter Eaat2. Astrocytes are critical regulators of glutamine and
309 glutamate homeostasis in the brain, which includes glutamate clearance from synapses, and
310 consequent regulation of glutamatergic neurotransmission and synaptic plasticity⁴⁹. There
311 were no convincing findings for the other cell classes examined.

312

313 **Shared gene dysregulation in heterozygous *Der1* cortex and t(1:11) translocation**
314 **carrier-derived cortical neuron cultures confirms the relevance of the *Der1* RNASeq**
315 **findings to psychiatric illness**

316 To determine how the above RNASeq data analyses of the *Der1* mouse relate to the t(1:11)
317 translocation, we compared the *Der1* mouse data to previously published RNASeq data
318 generated from t(1:11) translocation carrier-derived neuron cultures¹². Human iPSC-derived
319 neurons grown in culture are not directly comparable to adult mouse brain tissue. Even so, a

320 trend towards enrichment for shared gene expression changes was evident from the 20
321 dysregulated genes in common between iPSC-derived cortical neuron cultures from t(1:11)
322 translocation carriers¹² and heterozygous *Der1* hippocampus (p=0.06, Supplementary Table
323 2c, d), while 511 genes are differentially expressed in both heterozygous *Der1* mouse cortex
324 and the iPSC-derived cortical neuron cultures (Supplementary Table 2a, b), demonstrating
325 significant enrichment (p=1e-14), and further validating the *Der1* mouse as an accurate
326 model for the effect of the t(1:11) translocation upon DISC1 expression. An overlapping set
327 of cellular functions were also identified in the human cortical neuron cultures and
328 heterozygous *Der1* mouse cortex (Table 1, Supplementary Table 4a, d). Moreover, for most
329 of the shared functions there is either significant enrichment or a trend towards enrichment
330 for a common set of differentially expressed genes (Table 1). This convergence indicates
331 that disruption of *DISC1* likely contributes substantially to the altered molecular pathways in
332 the human neuron cultures.

333 Nonetheless, several functions are enriched in the *Der1* cortex data, but not in the
334 human cortical neuron data. Many relate specifically to synaptic plasticity and LTP,
335 processes that are constitutive in brain, but which require stimulation to be detected in
336 neuronal cultures. A number of other changes relate specifically to development of
337 dendrites, which may not reach maturity in iPSC-derived neuronal cultures⁵⁰.

338

339 **Mass spectrometry and SynGO analysis of adult *Der1* synaptosomes confirm synaptic** 340 **changes**

341 To complement the RNASeq analysis, synaptosome fractions were prepared from hetero- or
342 homozygous *Der1* mice and mass spectrometry was used to determine whether
343 synaptosomal protein expression profiles differ between mutant and wild-type mice. Of the
344 2,783 detected proteins in cortex, no changes survived multiple correction testing in
345 synaptosomes prepared from *Der1* mice (Supplementary Table 7a, Supplementary Figure
346 11). Of the 2,183 proteins detected in hippocampus, 62 were found to be dysregulated in
347 homozygotes (FDR adjusted p-value < 0.05, Supplementary Table 7b, Supplementary

348 Figure 11). These proteins were annotated to well-established synaptic genes using the
349 SynGO database⁵¹ (Figure 2c, Supplementary Table 7c). This is an expert-curated database
350 of gene ontology terms relating to synapses. From the 62 regulated proteins, 26 were found
351 annotated in SynGO, 24 with cellular component annotation and 19 with biological
352 processes annotation. Dysregulated proteins were found annotated across a wide spectrum
353 of pre- and post-synapse functions. For instance, several proteins were annotated to the
354 postsynaptic density, such as Camk2a (downregulated); AMPA receptor subunits
355 (downregulated); the DISC1 interactor Trio⁵², which modulates AMPA receptor currents in
356 hippocampal CA1 pyramidal neurons⁵³; vesicle proteins Exoc4, an exocyst component, and
357 the SNARE STX7; and Gad2, a presynaptic protein that synthesises GABA in interneurons.
358 These changes point to effects upon similar synaptic processes to those highlighted by
359 RNASeq analysis. However, fewer changes were detected in the synaptosomes, probably
360 due to the lower number of proteins identified in comparison with the RNASeq analysis, in
361 which many relevant RNASeq changes were detected at the isoform level.

362

363 **Functional effects of the *Der1* mutation upon synapses**

364 The RNAseq data point towards effects of the *Der1* mutation upon synapses, which was
365 confirmed by subsequent synaptic proteomics analysis. The observed changes include
366 subtly altered expression of NMDA receptor isoforms and reduced AMPA receptor subunit
367 levels. Moreover, we previously demonstrated that cultured hippocampal neuron dynamics
368 and cell surface/synaptic expression of NMDA receptors are dysregulated by the *Der1*
369 mutation¹².

370 To examine these receptors functionally, whole cell patch-clamping was used to
371 record currents from both receptor types in mature cultured hippocampal neurons (Figure
372 2d). The AMPA:NMDA ratio is decreased in homozygous *Der1* neurons indicating functional
373 imbalance between these two receptor subtypes. This may be due in part to altered AMPA
374 receptor currents, which although not statistically significant, are decreased in hetero- and
375 homozygous neurons. To discover whether this whole cell patch-clamp finding extends to

376 receptors located at synapses in heterozygous *Der1* hippocampus, and in cortex, will require
377 future in-depth electrophysiological measurements. If it does indeed extend to synapses, the
378 decreased AMPA:NMDA ratio could have many consequences including impaired triggering
379 of NMDA receptor-dependent LTP, which is initiated by AMPA receptor-induced release of
380 the magnesium block on NMDA receptors.

381

382 **Enrichment for dysregulation of putative schizophrenia, bipolar disorder and** 383 **depression risk genes in heterozygous *Der1* cortex and hippocampus**

384 A large number of putative schizophrenia risk genes have been identified from two large-
385 scale GWAS and one large-scale CNV study¹⁻³. IPA maps many of these genes to shared
386 molecular pathways. The top canonical pathway (Figure 3a) is 'CREB signalling in neurons'.
387 Others include 'Synaptic long-term potentiation' and 'Synaptic long-term depression', both
388 mechanisms underlying synaptic plasticity. These findings largely agree with previous
389 observations⁵⁴.

390 The heterozygous *Der1* cortex combined RNASeq DESeq2 plus DEXSeq data were
391 compared to the list of putative schizophrenia risk genes used above^{1,2}, but including only
392 genes encoding synaptic proteins from the CNV study³ as defined by its authors. This
393 identified significant enrichment for dysregulation of schizophrenia candidate gene
394 orthologues (Table 2, Supplementary Table 2a, b). The top canonical pathways identified
395 using this set of genes for IPA are 'Synaptic long-term depression', 'CREB signalling in
396 neurons', 'Synaptic long-term potentiation' and 'Calcium signalling' (Figure 3a-c). These
397 predictions are among the top five of those obtained using the full set of putative
398 schizophrenia risk genes (Figure 3a), indicating that the *Der1* mutation and genetic risk
399 factors for schizophrenia converge upon the same pathways.

400 Enrichment for dysregulation of schizophrenia candidate gene orthologues was also
401 apparent using the heterozygous *Der1* hippocampus combined RNAseq DESeq2 plus
402 DEXSeq data (Table 2, Supplementary Table 2c, d), although there were too few genes to
403 carry out meaningful pathway analysis.

404 Large-scale genetic data are also available for bipolar disorder and depression⁴⁻⁶.
405 IPA did not find that the genes identified from these studies converge strongly upon any
406 canonical pathways, although a subset of depression-associated genes are involved in
407 synaptic structure and activity⁶. Nonetheless, there is enrichment for dysregulation of the
408 orthologues of candidate genes for both disorders in *Der1* cortex, and for depression in *Der1*
409 hippocampus (Table 2, Supplementary Table 2). Moreover, the dysregulated putative
410 depression risk gene orthologues in *Der1* cortex predict effects upon the ‘CREB signalling in
411 neurons’ pathway (Figure 3a).

412 We also examined overlaps between genes dysregulated in the *Der1* mouse and two
413 non-psychiatric illness related large-scale GWAS. For Alzheimer’s Disease⁵⁵ there is
414 enrichment for dysregulation of candidate gene orthologues in *Der1* cortex (Table 2,
415 Supplementary Table 2), with six of the nine gene matches (ABCA7, APOE, CLU, FERMT2,
416 PTK2B/PYK2, SORL1) involved in Amyloid-Beta (A β)-related processes⁵⁶⁻⁶¹. This effect may
417 be explained by observations that DISC1 interacts with Amyloid Precursor Protein⁶², and
418 regulates A β generation^{63, 64}. The second comparison was to a study of cerebral cortex
419 architecture⁶⁵. Again, there is enrichment for dysregulation of candidate gene orthologues in
420 *Der1* cortex (Table 2, Supplementary Table 2), although no molecular pathways are
421 highlighted.

422 The enrichment for dysregulation of orthologues of candidate genes for brain
423 disorders (which is particularly striking for schizophrenia) when combined with convergence
424 upon specific molecular pathways already implicated in those disorders, indicates that the
425 *Der1* mutation may exert effects that are directly relevant to these human brain illnesses.

426

427 **Discussion**

428 Heterozygous *Der1* mutant mice accurately recapitulate the effects of the t(1:11)
429 translocation upon DISC1 expression in iPSC-derived neural precursors and cortical
430 neurons¹². We now demonstrate that patterns of gene expression dysregulation and

431 pathway predictions are similar between heterozygous *Der1* cortex, and iPSC-derived
432 cortical neuronal cultures from t(1:11) translocation carriers. Together these observations
433 suggest that *DISC1* disruption is an important factor in the increased risk of major mental
434 illness displayed by t(1:11) translocation carriers, and argue that the *Der1* mouse model can
435 be used to study the neuronal effects of *DISC1* disruption upon brain function to understand
436 disease mechanisms in these individuals.

437 Many of the findings reported here are consistent with known DISC1 biology and
438 brain function, but observations such as the lack of overt brain structural changes, and of
439 increased density of hippocampal Parvalbumin-expressing interneurons were unexpected on
440 the basis of previously described DISC1 mutant mice which model aspects of the effects of
441 the t(1;11) translocation upon DISC1 expression³⁵ (Supplementary Table 8). Such
442 differences, and the many phenotypic differences between previously published mutants
443 (Supplementary Table 8), accentuate the critical importance of studying a mutant that
444 accurately mimics all effects of the t(1;11) translocation in order to understand disease
445 mechanisms in t(1;11) translocation carriers. Other findings, such as the predicted
446 dysregulation of astrocyte lipid metabolism, have not been reported previously. This is the
447 first, and only, mutant mouse to accurately model effects of the t(1:11) translocation, and it
448 therefore provides important and new insights into molecular mechanisms underlying the
449 increased disease risk and psychiatric symptoms of t(1:11) translocation carriers.

450 Structural and functional brain abnormalities have been reported in human t(1:11)
451 translocation carriers¹¹, whereas none were detected in the adult *Der1* mice studied here.
452 This difference may reflect fundamental species differences in brain structure and
453 development, and/or secondary genetic or environmental factors consequent upon, or
454 interacting with, the t(1:11) translocation event. Genetic effects may include loss of normal
455 function of the additional disrupted genes *DISC2* and *DISC1FP1*^{13, 29}, or an influence of
456 genetic modifiers²⁸. Environmental effects may include greater relative age, and duration of
457 chronic mental illness with associated long-term exposure to medication such as

458 antipsychotic drugs. The latter progressively decreases grey matter volume in schizophrenia
459 patients⁶⁶, and decreases cortical volume in rats⁶⁷.

460 The absence of brain structural changes, together with the lack of evidence for
461 altered cell class proportions from RNASeq data deconvolution, indicates that the subtle
462 transcriptomic and proteomic alterations identified in the *Der1* mouse are principally due to
463 altered cellular properties that are largely conserved between it and t(1:11) translocation
464 carriers. EWCE analysis of RNASeq data suggests that the *Der1* mutation may target
465 distinct cell types including pyramidal neurons (CA1 and somatosensory) and interneurons.
466 These findings correlate well with a previous EWCE analysis using large-scale
467 schizophrenia GWAS data^{2, 34} which found that schizophrenia-associated SNPs map to
468 genomic loci containing genes that are highly expressed in a limited number of brain cell
469 types including CA1 and somatosensory pyramidal neurons, and interneurons³⁴, thus
470 implicating these cell types in the aetiology of schizophrenia. The additional cell types that
471 appear to be targeted by the *Der1* mutation: dopaminergic neurons, oxytocin/vasopressin-
472 expressing neurons and astrocytes/ependymocytes, were not implicated in schizophrenia by
473 the genomic EWCE analysis. However, dopamine signalling is heavily implicated in
474 schizophrenia, in part because all antipsychotic drugs in clinical use target the dopamine D2
475 receptor⁶⁸, while *DRD2* is located at a genetic locus repeatedly found to associate with
476 schizophrenia^{1, 2} and also with depression⁶. The neuropeptides oxytocin and vasopressin
477 regulate many processes, including social behaviour and anxiety⁶⁹, and are widely
478 implicated in psychiatric disorders⁷⁰. Astrocyte abnormalities have also been reported in
479 relation to psychiatric disorders⁷¹. Thus, even if not directly targeted by genomic risk
480 variants, these additional cell types do apparently contribute to psychiatric illness.

481 Pyramidal neurons are the major excitatory neurons in the brain. Interneurons are
482 inhibitory and regulate neuronal network excitability, primarily of pyramidal neurons. Our
483 analyses suggest widespread targeting of pyramidal neurons and interneurons by the *Der1*
484 mutation, thus excitation and inhibitory control of neuronal networks may be impaired.
485 Neuronal activity could be further impaired if the EWCE predictions are correct and

486 glutamate uptake by astrocytes is dysregulated. Our findings and predictions relating to
487 pyramidal neurons, which are glutamatergic cells, and to astrocytic glutamate uptake, may
488 be related to the decreased glutamate levels detected by brain imaging of t(1:11)
489 translocation carriers⁹. Altered lipid production by astrocytes may be an additional factor
490 affecting neuronal activity. Lipids are required for many processes, including synaptic
491 activity⁴⁷ and myelination⁴⁸. We have previously demonstrated impaired myelination in *Der1*
492 cortex which is presumably due, at least partially, to direct effects of the mutation upon
493 oligodendrocytes because the corresponding iPSC-derived oligodendrocytes from t(1:11)
494 translocation carriers are abnormal⁴⁶. EWCE analysis did not, however, find evidence that
495 oligodendrocytes are strongly targeted by the *Der1* mutation, although some genes highly
496 specific for this cell type are dysregulated, such as Myelin-Oligodendrocyte-Glycoprotein in
497 cortex (Supplementary Table 2a), while genes that impact myelination are dysregulated in
498 hippocampus (Supplementary Table 4b, 5). Altered lipid production by astrocytes could
499 therefore be a contributory factor in the myelination phenotype.

500 Consistent with the targeting of cell types implicated in schizophrenia, the *Der1*
501 mutation dysregulates orthologues of many genes implicated as risk factors for
502 schizophrenia and depressive disorders through large-scale genome-wide association and
503 CNV studies, as we have previously shown for the t(1:11) translocation in iPSC-derived
504 neurons¹². The pathways by which the t(1:11) translocation causes major mental illness may
505 therefore overlap those targeted by common genetic risk factors for schizophrenia and
506 depression. We speculate that disruption of the gene encoding the molecular scaffold
507 DISC1, with knock-on effects for its numerous binding partners and functions can, at least
508 partially, recapitulate the consequences of the more common scenario in psychiatric patients
509 whereby multiple interacting common genetic risk factors are inherited, with both scenarios
510 converging upon the same biological pathways. In agreement with this, the symptoms of
511 t(1:11) translocation carriers are indistinguishable from the typical spectrum of clinical
512 presentation of the psychiatric disorders with which they are diagnosed.

513 The convergence of the *Der1* mutation with a subset of putative common genetic risk
514 factors for schizophrenia and depressive disorders, and the convergence of this subset of
515 genes upon synapses and synaptic plasticity^{6, 54} implies that, of all the *Der1* cortex pathway
516 predictions, dysregulated neurotransmission and synaptic plasticity are among the most
517 critical factors in the psychiatric symptoms of t(1:11) translocation carriers. Notably, synaptic
518 plasticity underpins cognition, which is characteristically impaired in schizophrenia.

519 Altogether, the EWCE and pathway analyses pointing to potential pyramidal
520 neuron and interneuron dysfunction in hippocampus; the evidence that the number of
521 apoptotic cells in CA1 may be increased; the higher density of hippocampal Parvalbumin-
522 positive interneurons; the extensive changes to synaptic protein expression in hippocampus
523 synaptosomes; and the electrophysiology data indicating reduced AMPA:NMDA ratio in
524 cultured hippocampal neurons, suggest that hippocampal circuits are especially sensitive to
525 the mutation, although effects upon other brain regions are also likely.

526 The hippocampus has multiple input/output pathways from/to other brain regions
527 which are regulated by various neurotransmitters. Hippocampal dysfunction in *Der1* mice
528 could thus have numerous extrinsic/intrinsic causes, and knock-on effects. CA1 pyramidal
529 neurons provide the major hippocampal output, including the hippocampal-to-PFC pathway
530 that regulates NMDA receptor-dependent LTP and cognition⁷². This pathway is widely
531 implicated in psychiatric disorders⁷². It is thus an exemplar of the mechanisms by which
532 *DISC1* disruption could confer susceptibility to major mental illness by bringing together the
533 diverse effects described here, and elsewhere^{12, 46}, in our studies of neural cells derived from
534 t(1:11) translocation carriers, and of the corresponding *Der1* mouse. Our findings thus
535 provide important insights into potential disease mechanisms involving specific molecular
536 pathways/functions and cell types in t(1:11) translocation carriers that are likely relevant to
537 schizophrenia and affective disorders in general.

538

539 **Acknowledgements**

540 We thank the t(1:11) translocation family members who have taken part in our research by
541 donating skin biopsies for reprogramming and production of neural cells. This work was
542 funded by MRC grant MR/J004367/1; Brain & Behavior Research Foundation Independent
543 Investigator Grant 23306 and Young Investigator Grant 27404; European Union Seventh
544 Framework Programme 607616FP7, Deciphering inter- and intracellular signalling in
545 schizophrenia; a bequest from Eva Lester; Scottish Funding Council Scottish Senior
546 Fellowship and Chief Scientists Office Senior Clinical fellowship Starter Grant awards to
547 AMM; the University of Edinburgh Wellcome Trust Institutional Support Fund grant J22734, a
548 Sir Henry Wellcome postdoctoral fellowship (213674/Z/18/Z) awarded to DMH;
549 EUREKA/European Union Eurostars E! 7675; and an NWO Gravitation project: A Roadmap
550 from Neurogenetics to Neurobiology (NWO: 024.004.0212).

551

552 **Conflict of interest statement**

553 The authors declare no competing financial interests. AMM has received research support
554 from Eli Lilly and Company, Janssen and the Sackler Trust, and speaker fees from Illumina
555 and Janssen. ACV has received research support from F. Hoffman La Roche and UCB
556 Biopharma SPRL. ML is a full time employee of Sylics (Synaptologics B.V.), a private
557 company that offers mouse phenotyping services. ABS is shareholder of Alea Biotech B.V.,
558 a holding of Sylics (Synaptologics B.V.). MD is based at Sanofi.

559 **Table 1** Top relevant altered cellular functions in heterozygous *Der1* mouse cortex and
560 human iPSC-derived neurons from members of the t(1;11) translocation family predicted
561 using DESeq2+DEXSeq data. All *Der1* mouse and human t(1;11) neuron functions are listed
562 in Supplementary Table 4.

Function (no. of molecules ^a)	<i>Der1</i> cortex score (no. of genes ^b)	Human t(1:11) translocation neuron culture score (no. of genes ^b)	Hypergeometric p value for enrichment (no. of shared genes ^c)
General cell morphology			
Development of neurons (1,423)	p=2e-53 (457)	p=2e-13 (148)	p=1e-3 (63)
Morphogenesis of neurons (1,080)	p=1e-47 (360)	p=4e-13 (119)	p=3e-4 (56)
Morphology of neurons (1,123)	p=7e-37 (303)	p=1e-4 (80)	p=6e-5 (37)
Morphology of cells (4,370)	p=1e-29 (902)		
Abnormal morphology of neurons (923)	p=6e-25 (212)		
Cell contact			
Cell-cell contact (1,118)	p=5e-26 (299)	p=4e-6 (92)	p=6e-4 (38)
Development of gap junctions (327)	p=1e-18 (123)	p=2e-4 (37)	p=0.08 (17)
Formation of cell-cell contacts (414)	p=6e-16 (138)	p=8e-6 (48)	p=0.08 (19)
Formation of intercellular junctions (409)	p=1e-15 (136)	p=1e-5 (47)	p=0.07 (19)
Formation of plasma membrane (406)	p=1e-15 (134)	p=3e-6 (48)	p=0.05 (20)
Cytoskeleton			
Organization of cytoplasm (2,832)	p=2e-64 (791)	p=3e-16 (257)	p=2e-6 (104)
Organization of cytoskeleton (2,624)	p=4e-57 (720)	p=3e-16 (240)	p=1e-8 (101)
Microtubule dynamics (2,247)	p=6e-54 (627)	p=1e-14 (206)	p=1e-6 (87)
Development of cytoplasm (873)	p=9e-19 (233)	p=2e-4 (71)	p=1e-5 (35)
Formation of cytoskeleton (733)	p=5e-14 (179)		
Cellular protrusions/neurites			
Neuritogenesis (1,067)	p=2e-46 (354)	p=4e-12 (115)	p=2e-4 (55)
Formation of cellular protrusions (1,645)	p=1e-46 (488)	p=3e-15 (170)	p=2e-4 (70)
Growth of neurites (910)	p=5e-30 (261)	p=1e-7 (81)	p=6e-4 (36)
Morphology of cellular protrusions (522)	p=3e-25 (166)		
Morphology of neurites (414)	p=6e-25 (139)		
Axons			
Axonogenesis (338)	p=1e-18 (122)	p=2e-7 (45)	p=2e-3 (25)
Morphology of axons (169)	p=2e-16 (65)		
Growth of axons (281)	p=2e-12 (87)		
Abnormal morphology of axons (133)	p=4e-11 (46)		
Guidance of axons (202)	p=5e-10 (71)	p=2e-5 (29)	ns (12)
Dendrites			
Formation of dendrites (209)	p=9e-19 (90)		
Dendritic growth/branching (446)	p=8e-18 (131)		
Density of dendritic spines (143)	p=1e-11 (49)		
Morphology of dendrites (138)	p=3e-9 (49)		
Abnormal morphology of dendrites (75)	p=3e-8 (32)		
Cell proliferation			
Proliferation of neuronal cells (1066)	p=5e-28 (290)	p=2e-9 (98)	p=2e-3 (39)
Neuronal migration			
Migration of neurons (362)	p=1e-16 (125)	p=8e-6 (43)	p=0.03 (20)
Circadian rhythm			
Circadian rhythm (132)	p=3e-8 (55)		
Transport			
Organisation of organelle (948)	p=1e-23 (270)		
Transport of vesicles (192)	p=1e-14 (69)		
Endocytosis (924)	p=8e-10 (202)	p=3e-6 (76)	p=2e-3 (27)
Secretory pathway (367)	p=8e-10 (93)		
Formation of vesicles (307)	p=4e-9 (70)		
Neurotransmission			
Neurotransmission (716)	p=5e-31 (233)	p=5e-5 (62)	p=0.03 (26)
Potentiation of synapse (546)	p=1e-28 (165)		
Long-term potentiation (539)	p=4e-28 (163)		
Synaptic transmission (558)	p=4e-27 (191)	p=7e-06 (55)	p=0.04 (24)
Developmental process of synapse (303)	p=2e-18 (117)	p=1e-4 (36)	p=0.08 (17)
Excitatory postsynaptic potential (166)	p=2e-15 (72)		
Long-term potentiation of brain (281)	p=2e-13 (74)		
Plasticity of synapse (170)	p=2e-12 (66)		

Long-term potentiation of cerebral cortex (254)	p=6e-12 (66)		
Miniature excitatory postsynaptic currents (71)	p=1e-11 (38)		

563

564

A full list of functions is provided in Supplementary Table 4a, d. Related functions are

565

grouped, with top functions shown for each group. a, total number of molecules relating to

566

each IPA function; b, number of dysregulated genes relating to each function; c, number of

567

genes relating to function that are dysregulated in both *Der1* cortex and human t(1:11)

568

translocation neurons; italics, trend; ns, not significant

569

570 **Table 2** Enrichment for dysregulated expression of putative psychiatric illness risk gene
 571 orthologues in *Der1* cortex and hippocampus.

Study	Loci	Genes	Dysregulated in cortex	Hypergeometric p value for enrichment in cortex	Dysregulated in hippocampus	Hypergeometric p value for enrichment in hippocampus
GWAS, schizophrenia ¹	108	348	121 genes at 61 loci	p=1e-13 (p=8e-19)	6 genes at 6 loci	p=0.04 (p=2e-4)
GWAS, schizophrenia ²	143	481	127 genes at 73 loci	p=3e-6 (p=8e-19)	6 genes at 6 loci	<i>p=0.09 (p=8e-4)</i>
MAGMA, schizophrenia ²		535	210	p=3e-30	15	p=2e-5
CNV (synapse genes), schizophrenia ³		52	25	p=8e-7	4	p=7e-4
GWAS, depression ⁴	44	70	19 at 19 loci	p=0.02 (p=9e-5)	1	ns
MAGMA, depression ⁴		153	33	p=0.047	1	ns
MAGMA meta-analysis, depression ⁵		269	94	p=4e-11	6	p=0.01
GWAS, bipolar disorder ⁵	30	218	73 at 21 loci	p=4e-8 (p=8e-10)	3 genes at 3 loci	ns (p=2e-3)
MAGMA, bipolar disorder ⁵		152	49	p=2e-5	3	<i>p=0.09</i>
GWAS, Alzheimer's Disease ⁵⁵	21	102	9 at 9 loci	p=3e-3 (p=6e-3)	1	ns
GWAS cerebral cortex architecture ⁶⁵		193	57	p=5e-5	1	ns

572

573 Loci indicates the number of associated genomic loci identified by GWAS. Genes indicates

574 the total number of genes at the associated loci, or the total number identified by MAGMA.

575 Bracketed p values indicate enrichment for loci containing at least one dysregulated gene

576 orthologue. italics, trend; ns, not significant

577

578 **References**

- 579 1. Schizophrenia Working Group of the Psychiatric Genomics C. Biological insights
580 from 108 schizophrenia-associated genetic loci. *Nature* 2014; **511**(7510): 421-427.
581
- 582 2. Pardinás AF, Holmans P, Pocklington AJ, Escott-Price V, Ripke S, Carrera N *et al.*
583 Common schizophrenia alleles are enriched in mutation-intolerant genes and in
584 regions under strong background selection. *Nature genetics* 2018; **50**(3): 381-389.
585
- 586 3. Cnv, Schizophrenia Working Groups of the Psychiatric Genomics C, Psychosis
587 Endophenotypes International C. Contribution of copy number variants to
588 schizophrenia from a genome-wide study of 41,321 subjects. *Nature genetics* 2017;
589 **49**(1): 27-35.
590
- 591 4. Wray NR, Ripke S, Mattheisen M, Trzaskowski M, Byrne EM, Abdellaoui A *et al.*
592 Genome-wide association analyses identify 44 risk variants and refine the genetic
593 architecture of major depression. *Nature genetics* 2018; **50**(5): 668-681.
594
- 595 5. Stahl EA, Breen G, Forstner AJ, McQuillin A, Ripke S, Trubetskoy V *et al.* Genome-
596 wide association study identifies 30 loci associated with bipolar disorder. *Nature*
597 *genetics* 2019; **51**(5): 793-803.
598
- 599 6. Howard DM, Adams MJ, Clarke TK, Hafferty JD, Gibson J, Shiralí M *et al.* Genome-
600 wide meta-analysis of depression identifies 102 independent variants and highlights
601 the importance of the prefrontal brain regions. *Nature neuroscience* 2019; **22**(3): 343-
602 352.

603

604 7. St Clair D, Blackwood D, Muir W, Carothers A, Walker M, Spowart G *et al.*
605 Association within a family of a balanced autosomal translocation with major mental
606 illness. *Lancet* 1990; **336**(8706): 13-16.

607

608 8. Blackwood DH, Fordyce A, Walker MT, St Clair DM, Porteous DJ, Muir WJ.
609 Schizophrenia and affective disorders--cosegregation with a translocation at
610 chromosome 1q42 that directly disrupts brain-expressed genes: clinical and P300
611 findings in a family. *American journal of human genetics* 2001; **69**(2): 428-433.

612

613 9. Thomson PA, Duff B, Blackwood DH, Romaniuk L, Watson A, Whalley HC *et al.*
614 Balanced translocation linked to psychiatric disorder, glutamate, and cortical
615 structure/function. *NPJ Schizophr* 2016; **2**: 16024.

616

617 10. Whalley HC, Dimitrova R, Sprooten E, Dauvermann MR, Romaniuk L, Duff B *et al.*
618 Effects of a Balanced Translocation between Chromosomes 1 and 11 Disrupting the
619 DISC1 Locus on White Matter Integrity. *PLoS One* 2015; **10**(6): e0130900.

620

621 11. Doyle OM, Bois C, Thomson P, Romaniuk L, Witcher B, Williams SC *et al.* The
622 cortical thickness phenotype of individuals with DISC1 translocation resembles
623 schizophrenia. *J Clin Invest* 2015; **125**(9): 3714-3722.

624

625 12. Malavasi ELV, Economides KD, Grunewald E, Makedonopoulou P, Gautier P,
626 Mackie S *et al.* DISC1 regulates N-methyl-D-aspartate receptor dynamics:
627 abnormalities induced by a Disc1 mutation modelling a translocation linked to major
628 mental illness. *Transl Psychiatry* 2018; **8**(1): 184.

629

630 13. Millar JK, Wilson-Annan JC, Anderson S, Christie S, Taylor MS, Semple CA *et al.*
631 Disruption of two novel genes by a translocation co-segregating with schizophrenia.
632 *Human molecular genetics* 2000; **9**(9): 1415-1423.

633

634 14. Camargo LM, Collura V, Rain JC, Mizuguchi K, Hermjakob H, Kerrien S *et al.*
635 Disrupted in Schizophrenia 1 Interactome: evidence for the close connectivity of risk
636 genes and a potential synaptic basis for schizophrenia. *Molecular psychiatry* 2007;
637 **12**(1): 74-86.

638

639 15. Brandon NJ, Millar JK, Korth C, Sive H, Singh KK, Sawa A. Understanding the role of
640 DISC1 in psychiatric disease and during normal development. *J Neurosci* 2009;
641 **29**(41): 12768-12775.

642

643 16. Mao Y, Ge X, Frank CL, Madison JM, Koehler AN, Doud MK *et al.* Disrupted in
644 schizophrenia 1 regulates neuronal progenitor proliferation via modulation of
645 GSK3beta/beta-catenin signaling. *Cell* 2009; **136**(6): 1017-1031.

646

647 17. Duan X, Chang JH, Ge S, Faulkner RL, Kim JY, Kitabatake Y *et al.* Disrupted-In-
648 Schizophrenia 1 regulates integration of newly generated neurons in the adult brain.
649 *Cell* 2007; **130**(6): 1146-1158.

650

651 18. Kamiya A, Kubo K, Tomoda T, Takaki M, Youn R, Ozeki Y *et al.* A schizophrenia-
652 associated mutation of DISC1 perturbs cerebral cortex development. *Nature cell*
653 *biology* 2005; **7**(12): 1167-1178.

654

- 655 19. Ogawa F, Malavasi EL, Crummie DK, Eykelenboom JE, Soares DC, Mackie S *et al.*
656 DISC1 complexes with TRAK1 and Miro1 to modulate anterograde axonal
657 mitochondrial trafficking. *Human molecular genetics* 2014; **23**(4): 906-919.
- 658
- 659 20. Atkin TA, MacAskill AF, Brandon NJ, Kittler JT. Disrupted in Schizophrenia-1
660 regulates intracellular trafficking of mitochondria in neurons. *Molecular psychiatry*
661 2011; **16**(2): 122-124, 121.
- 662
- 663 21. Flores R, 3rd, Hirota Y, Armstrong B, Sawa A, Tomoda T. DISC1 regulates synaptic
664 vesicle transport via a lithium-sensitive pathway. *Neurosci Res* 2011; **71**(1): 71-77.
- 665
- 666 22. Tsuboi D, Kuroda K, Tanaka M, Namba T, Iizuka Y, Taya S *et al.* Disrupted-in-
667 schizophrenia 1 regulates transport of ITPR1 mRNA for synaptic plasticity. *Nature*
668 *neuroscience* 2015; **18**(5): 698-707.
- 669
- 670 23. Wei J, Graziane NM, Gu Z, Yan Z. DISC1 Protein Regulates gamma-Aminobutyric
671 Acid, Type A (GABAA) Receptor Trafficking and Inhibitory Synaptic Transmission in
672 Cortical Neurons. *The Journal of biological chemistry* 2015; **290**(46): 27680-27687.
- 673
- 674 24. Wei J, Graziane NM, Wang H, Zhong P, Wang Q, Liu W *et al.* Regulation of N-
675 Methyl-D-Aspartate Receptors by Disrupted-in-Schizophrenia-1. *Biological psychiatry*
676 2013.
- 677
- 678 25. Wen Z, Nguyen HN, Guo Z, Lalli MA, Wang X, Su Y *et al.* Synaptic dysregulation in a
679 human iPS cell model of mental disorders. *Nature* 2014.

680

681 26. Tropea D, Molinos I, Petit E, Bellini S, Nagakura I, O'Tuathaigh C *et al.* Disrupted in
682 schizophrenia 1 (DISC1) L100P mutants have impaired activity-dependent plasticity
683 in vivo and in vitro. *Transl Psychiatry* 2016; **6**: e712.

684

685 27. Zhou X, Geyer MA, Kelsoe JR. Does disrupted-in-schizophrenia (DISC1) generate
686 fusion transcripts? *Molecular psychiatry* 2008; **13**(4): 361-363.

687

688 28. Ryan NM, Lihm J, Kramer M, McCarthy S, Morris SW, Arnau-Soler A *et al.* DNA
689 sequence-level analyses reveal potential phenotypic modifiers in a large family with
690 psychiatric disorders. *Molecular psychiatry* 2018.

691

692 29. Eykelenboom JE, Briggs GJ, Bradshaw NJ, Soares DC, Ogawa F, Christie S *et al.* A
693 t(1;11) translocation linked to schizophrenia and affective disorders gives rise to
694 aberrant chimeric DISC1 transcripts that encode structurally altered, deleterious
695 mitochondrial proteins. *Human molecular genetics* 2012; **21**(15): 3374-3386.

696

697 30. Tropea D, Hardingham N, Millar K, Fox K. Mechanisms underlying the role of DISC1
698 in synaptic plasticity. *The Journal of physiology* 2018; **596**(14): 2747-2771.

699

700 31. Love MI, Huber W, Anders S. Moderated estimation of fold change and dispersion for
701 RNA-seq data with DESeq2. *Genome biology* 2014; **15**(12): 550.

702

703 32. Anders S, Reyes A, Huber W. Detecting differential usage of exons from RNA-seq
704 data. *Genome Res* 2012; **22**(10): 2008-2017.

705

706 33. Skene NG, Grant SG. Identification of Vulnerable Cell Types in Major Brain Disorders
707 Using Single Cell Transcriptomes and Expression Weighted Cell Type Enrichment.
708 *Front Neurosci* 2016; **10**: 16.

709

710 34. Skene NG, Bryois J, Bakken TE, Breen G, Crowley JJ, Gaspar HA *et al.* Genetic
711 identification of brain cell types underlying schizophrenia. *Nature genetics* 2018;
712 **50**(6): 825-833.

713

714 35. Brandon NJ, Sawa A. Linking neurodevelopmental and synaptic theories of mental
715 illness through DISC1. *Nature reviews* 2011; **12**(12): 707-722.

716

717 36. Newman AM, Liu CL, Green MR, Gentles AJ, Feng W, Xu Y *et al.* Robust
718 enumeration of cell subsets from tissue expression profiles. *Nat Methods* 2015;
719 **12**(5): 453-457.

720

721 37. Park YU, Jeong J, Lee H, Mun JY, Kim JH, Lee JS *et al.* Disrupted-in-schizophrenia
722 1 (DISC1) plays essential roles in mitochondria in collaboration with Mitofilin.
723 *Proceedings of the National Academy of Sciences of the United States of America*
724 2010; **107**(41): 17785-17790.

725

726 38. Pinero-Martos E, Ortega-Vila B, Pol-Fuster J, Cisneros-Barroso E, Ruiz-Guerra L,
727 Medina-Dols A *et al.* Disrupted in schizophrenia 1 (DISC1) is a constituent of the
728 mammalian mitochondrial contact site and cristae organizing system (MICOS)
729 complex, and is essential for oxidative phosphorylation. *Human molecular genetics*
730 2016.

731

732 39. Wang Q, Charych EI, Pulito VL, Lee JB, Graziane NM, Crozier RA *et al.* The
733 psychiatric disease risk factors DISC1 and TNK1 interact to regulate synapse
734 composition and function. *Molecular psychiatry* 2011; **16**(10): 1006-1023.

735

736 40. Jaaro-Peled H, Altimus C, LeGates T, Cash-Padgett T, Zoubovsky S, Hikida T *et al.*
737 Abnormal wake/sleep pattern in a novel gain-of-function model of DISC1. *Neurosci*
738 *Res* 2016; **112**: 63-69.

739

740 41. Seshadri S, Faust T, Ishizuka K, Delevich K, Chung Y, Kim SH *et al.* Interneuronal
741 DISC1 regulates NRG1-ErbB4 signalling and excitatory-inhibitory synapse formation
742 in the mature cortex. *Nat Commun* 2015; **6**: 10118.

743

744 42. Tang W, Thevathasan JV, Lin Q, Lim KB, Kuroda K, Kaibuchi K *et al.* Stimulation of
745 Synaptic Vesicle Exocytosis by the Mental Disease Gene DISC1 is Mediated by N-
746 Type Voltage-Gated Calcium Channels. *Front Synaptic Neurosci* 2016; **8**: 15.

747

748 43. Hattori T, Shimizu S, Koyama Y, Yamada K, Kuwahara R, Kumamoto N *et al.* DISC1
749 regulates cell-cell adhesion, cell-matrix adhesion and neurite outgrowth. *Molecular*
750 *psychiatry* 2010; **15**(8): 778, 798-809.

751

752 44. Shimizu S, Koyama Y, Hattori T, Tachibana T, Yoshimi T, Emoto H *et al.* DBZ, a
753 CNS-specific DISC1 binding protein, positively regulates oligodendrocyte
754 differentiation. *Glia* 2014; **62**(5): 709-724.

755

- 756 45. Hattori T, Shimizu S, Koyama Y, Emoto H, Matsumoto Y, Kumamoto N *et al.* DISC1
757 (disrupted-in-schizophrenia-1) regulates differentiation of oligodendrocytes. *PLoS*
758 *One* 2014; **9**(2): e88506.
- 759
- 760 46. Vasistha NA, Johnstone M, Barton SK, Mayerl SE, Thangaraj Selvaraj B, Thomson
761 PA *et al.* Familial t(1;11) translocation is associated with disruption of white matter
762 structural integrity and oligodendrocyte-myelin dysfunction. *Molecular psychiatry*
763 2019.
- 764
- 765 47. van Deijk AF, Camargo N, Timmerman J, Heistek T, Brouwers JF, Mogavero F *et al.*
766 Astrocyte lipid metabolism is critical for synapse development and function in vivo.
767 *Glia* 2017; **65**(4): 670-682.
- 768
- 769 48. Camargo N, Goudriaan A, van Deijk AF, Otte WM, Brouwers JF, Lodder H *et al.*
770 Oligodendroglial myelination requires astrocyte-derived lipids. *PLoS Biol* 2017; **15**(5):
771 e1002605.
- 772
- 773 49. Mahan VL. Neurointegrity and neurophysiology: astrocyte, glutamate, and carbon
774 monoxide interactions. *Med Gas Res* 2019; **9**(1): 24-45.
- 775
- 776 50. Prytkova I, Brennand KJ. Prospects for Modeling Abnormal Neuronal Function in
777 Schizophrenia Using Human Induced Pluripotent Stem Cells. *Front Cell Neurosci*
778 2017; **11**: 360.
- 779

- 780 51. Koopmans F, van Nierop P, Andres-Alonso M, Byrnes A, Cijssouw T, Coba MP *et al.*
781 SynGO: An Evidence-Based, Expert-Curated Knowledge Base for the Synapse.
782 *Neuron* 2019; **103**(2): 217-234 e214.
- 783
- 784 52. Chen SY, Huang PH, Cheng HJ. Disrupted-in-Schizophrenia 1-mediated axon
785 guidance involves TRIO-RAC-PAK small GTPase pathway signaling. *Proceedings of*
786 *the National Academy of Sciences of the United States of America* 2011; **108**(14):
787 5861-5866.
- 788
- 789 53. Ba W, Yan Y, Reijnders MR, Schuurs-Hoeijmakers JH, Feenstra I, Bongers EM *et al.*
790 TRIO loss of function is associated with mild intellectual disability and affects
791 dendritic branching and synapse function. *Human molecular genetics* 2016; **25**(5):
792 892-902.
- 793
- 794 54. Hall J, Trent S, Thomas KL, O'Donovan MC, Owen MJ. Genetic risk for
795 schizophrenia: convergence on synaptic pathways involved in plasticity. *Biological*
796 *psychiatry* 2015; **77**(1): 52-58.
- 797 55. Kunkle BW, Grenier-Boley B, Sims R, Bis JC, Damotte V, Naj AC *et al.* Genetic
798 meta-analysis of diagnosed Alzheimer's disease identifies new risk loci and
799 implicates Abeta, tau, immunity and lipid processing. *Nature genetics* 2019; **51**(3):
800 414-430.
- 801
- 802 56. Sakae N, Liu CC, Shinohara M, Frisch-Daiello J, Ma L, Yamazaki Y *et al.* ABCA7
803 Deficiency Accelerates Amyloid-beta Generation and Alzheimer's Neuronal
804 Pathology. *J Neurosci* 2016; **36**(13): 3848-3859.
- 805

- 806 57. Holtzman DM. Role of apoe/Abeta interactions in the pathogenesis of Alzheimer's
807 disease and cerebral amyloid angiopathy. *J Mol Neurosci* 2001; **17**(2): 147-155.
808
- 809 58. Li X, Ma Y, Wei X, Li Y, Wu H, Zhuang J *et al.* Clusterin in Alzheimer's disease: a
810 player in the biological behavior of amyloid-beta. *Neurosci Bull* 2014; **30**(1): 162-168.
811
- 812 59. Chapuis J, Flaig A, Grenier-Boley B, Eysert F, Pottiez V, Deloison G *et al.* Genome-
813 wide, high-content siRNA screening identifies the Alzheimer's genetic risk factor
814 FERMT2 as a major modulator of APP metabolism. *Acta neuropathologica* 2017;
815 **133**(6): 955-966.
816
- 817 60. Salazar SV, Cox TO, Lee S, Brody AH, Chyung AS, Haas LT *et al.* Alzheimer's
818 Disease Risk Factor Pyk2 Mediates Amyloid-beta-Induced Synaptic Dysfunction and
819 Loss. *J Neurosci* 2019; **39**(4): 758-772.
820
- 821 61. Alexopoulos P, Kurz A, Lewczuk P, Kornhuber J, Wiltfang J, Maier W *et al.* The
822 sortilin-related receptor SORL1 and the amyloid cascade: a possible explanation for
823 the concurrent elevation of CSF soluble APPalpha and APPbeta in Alzheimer's
824 disease. *Int J Geriatr Psychiatry* 2010; **25**(5): 542-543.
825
- 826 62. Young-Pearse TL, Suth S, Luth ES, Sawa A, Selkoe DJ. Biochemical and functional
827 interaction of disrupted-in-schizophrenia 1 and amyloid precursor protein regulates
828 neuronal migration during mammalian cortical development. *J Neurosci* 2010;
829 **30**(31): 10431-10440.
830

- 831 63. Shahani N, Seshadri S, Jaaro-Peled H, Ishizuka K, Hirota-Tsuyada Y, Wang Q *et al.*
832 DISC1 regulates trafficking and processing of APP and Abeta generation. *Molecular*
833 *psychiatry* 2015; **20**(7): 874-879.
- 834
- 835 64. Deng QS, Dong XY, Wu H, Wang W, Wang ZT, Zhu JW *et al.* Disrupted-in-
836 Schizophrenia-1 Attenuates Amyloid-beta Generation and Cognitive Deficits in
837 APP/PS1 Transgenic Mice by Reduction of beta-Site APP-Cleaving Enzyme 1
838 Levels. *Neuropsychopharmacology* 2016; **41**(2): 440-453.
- 839
- 840 65. Grasby KL, Jahanshad N, Painter JN, Colodro-Conde L, Bralten J, Hibar DP *et al.*
841 The genetic architecture of the human cerebral cortex. *Science (New York, NY* 2020;
842 **367**(6484).
- 843
- 844 66. Fusar-Poli P, Smieskova R, Kempton MJ, Ho BC, Andreasen NC, Borgwardt S.
845 Progressive brain changes in schizophrenia related to antipsychotic treatment? A
846 meta-analysis of longitudinal MRI studies. *Neurosci Biobehav Rev* 2013; **37**(8): 1680-
847 1691.
- 848
- 849 67. Vernon AC, Crum WR, Lerch JP, Chege W, Natesan S, Modo M *et al.* Reduced
850 cortical volume and elevated astrocyte density in rats chronically treated with
851 antipsychotic drugs-linking magnetic resonance imaging findings to cellular
852 pathology. *Biological psychiatry* 2014; **75**(12): 982-990.
- 853
- 854 68. Sonnenschein SF, Grace AA. Insights on current and novel antipsychotic
855 mechanisms from the MAM model of schizophrenia. *Neuropharmacology* 2019.
- 856

- 857 69. Bredewold R, Veenema AH. Sex differences in the regulation of social and anxiety-
858 related behaviors: insights from vasopressin and oxytocin brain systems. *Curr Opin*
859 *Neurobiol* 2018; **49**: 132-140.
- 860
- 861 70. Iovino M, Messana T, De Pergola G, Iovino E, Dicuonzo F, Guastamacchia E *et al.*
862 The Role of Neurohypophyseal Hormones Vasopressin and Oxytocin in
863 Neuropsychiatric Disorders. *Endocr Metab Immune Disord Drug Targets* 2018; **18**(4):
864 341-347.
- 865
- 866 71. Elsayed M, Magistretti PJ. A New Outlook on Mental Illnesses: Glial Involvement
867 Beyond the Glue. *Front Cell Neurosci* 2015; **9**: 468.
- 868
- 869 72. Godsil BP, Kiss JP, Spedding M, Jay TM. The hippocampal-prefrontal pathway: the
870 weak link in psychiatric disorders? *Eur Neuropsychopharmacol* 2013; **23**(10): 1165-
871 1181.
- 872
- 873 73. Pandya NJ, Koopmans F, Slotman JA, Paliukhovich I, Houtsmuller AB, Smit AB *et al.*
874 Correlation profiling of brain sub-cellular proteomes reveals co-assembly of synaptic
875 proteins and subcellular distribution. *Sci Rep* 2017; **7**(1): 12107.
- 876

877 **Legends to figures**

878 **Fig. 1** The *Der1* mutation targets specific cell types in heterozygous cortex and
879 hippocampus. **a** *Disc1* RNASeq reads normalised to total reads per sample in wild-type
880 versus heterozygous *Der1* cortex and hippocampus. **b** Heat maps of the top 500
881 dysregulated genes identified by RNASeq of wild-type versus heterozygous *Der1* cortex and
882 hippocampus. **c d** EWCE analysis of heterozygous *Der1* cortex and hippocampus,
883 respectively, in mouse brain cell classes. asterisk, significance after Bonferroni correction;
884 Emb, embryonic; Hyp, hypothalamic; SD, standard deviation **e** Parvalbumin expression in
885 hippocampal sections from nine week old mouse brain. Enlarged regions showing
886 Parvalbumin-expressing interneurons are indicated by boxes. scale bars, 100µm **f** Average
887 density of Parvalbumin-expressing interneurons. Hippocampus refers to the whole
888 hippocampal formation. Data were analysed by Kruskal-Wallis one-way ANOVA, $p=0.07$ for
889 the dentate gyrus; $p=0.049$ for the hippocampal formation. Horizontal line on graphs for each
890 sample, average of values; WT, wild-type; HET, heterozygous *Der1*; HOM, homozygous
891 *Der1*; DG, dentate gyrus; *, $p<0.05$

892

893 **Fig. 2** Consequences of the *Der1* mutation. **a** Top relevant canonical pathway predictions for
894 heterozygous *Der1* cortex using whole gene, DESeq2, or whole gene and exon level,
895 DESeq2+DEXSeq data. Asterisks indicate pathways highlighted in both cases. Where IPA
896 predicts a direction of change this is indicated by a z score, with positive z scores indicating
897 upregulation. **b** Altered gene expression in the 'CREB signalling in neurons' canonical
898 pathway in heterozygous *Der1* cortex, determined using whole gene and exon level
899 DESeq2+DEXSeq data. To provide additional information, genes encoding calcium channels
900 (CaCh), metabotropic glutamate receptors (mGLUR), ionotropic glutamate receptor subunits
901 (iGLUR) and structural synaptic components have been added to the pathway using the IPA
902 'Build' tool. Transcripts encoding components from the whole pathway are dysregulated at
903 the whole gene and/or isoform level, including ionotropic AMPA and NMDA glutamate
904 receptor subunits, metabotropic glutamate receptors and voltage-gated calcium channels, all

905 of which can control the calcium ion influx or G-protein activation that initiates the pathway.
906 Genes encoding several synaptic scaffolds that are required to generate and maintain
907 synapse structure/size and/or anchor glutamate receptors and calcium channels are also
908 dysregulated, including Shank1, Homer1 and Dlg1/3/4, neuroligins and neuroligins. Also
909 dysregulated are genes encoding various factors downstream of glutamate receptors and
910 calcium channels that activate the cAMP-dependent transcription factor CREB, such as
911 various forms of Camk2, and adenylyl cyclases. The transcriptional machinery is additionally
912 affected, including the cAMP-dependent transcription factor complex. Double outlines
913 indicate protein complexes and classes, the components of which can be found in
914 Supplementary Table 2a, b. Colour intensity represents strength of gene expression change,
915 with graded colour within double outlined symbols representing overall direction of change
916 within protein complexes. green, downregulated; red, upregulated; *genes identified by
917 DEXSeq; ** genes identified by DEXSeq and DESeq2 **c** Sunburst plots showing SynGO
918 annotated synaptic functions of the dysregulated proteins found in homozygous *Der1*
919 hippocampus synaptosomes (FDR adjusted p-value < 0.05). Note that synaptosomes are
920 enriched for the complete presynaptic terminal, the postsynaptic membrane and the
921 postsynaptic density, as well as membranes originating from organelles such as the Golgi
922 and endoplasmic reticulum⁷³. **d** Quantification of AMPA and NMDA receptor currents by
923 whole-cell patch clamping of neurons cultured from *Der1* hippocampus. Data were analysed
924 by one-way ANOVA, p=0.03. Horizontal line on graphs for each sample, average of values;
925 WT, wild-type; HET, heterozygous *Der1*; HOM, homozygous *Der1*; *, p<0.05

926

927 **Fig. 3** The *Der1* mutation dysregulates canonical pathways and genes related to
928 schizophrenia and depression in heterozygous *Der1* cortex. **a** Canonical pathway predictions
929 for putative schizophrenia risk genes, and for orthologues of putative schizophrenia and
930 depression risk genes that are dysregulated at the whole gene and exon level, as identified
931 using DESeq2+DEXSeq data. **b, c** Altered schizophrenia risk gene orthologue expression in
932 the 'Synaptic long-term depression' and 'CREB signalling in neurons' canonical pathways,

933 respectively. Double outlines indicate protein complexes and classes, the components of
934 which can be found in Supplementary Table 2a, b. To provide additional information, genes
935 encoding ionotropic glutamate receptor δ subunits (Grid), AMPA receptor subunits (AMPA),
936 voltage-gated calcium channel subunits (VGCC), calcium channels (CaCh), ionotropic
937 glutamate receptor subunits (iGLUR) and structural synaptic components have been added
938 to the pathways using the IPA 'Build' tool. *genes identified by DEXSeq; red, dysregulated
939 putative schizophrenia risk gene orthologue

940

941 **Functional brain defects in a mouse model of a chromosomal t(1;11) translocation**
942 **that disrupts *DISC1* and confers increased risk of psychiatric illness**

943

944 **Supplementary information**

945

946 Marion Bonneau¹, Shane T. O'Sullivan¹, Miguel A. Gonzalez-Lozano², Paul Baxter³,
947 Phillippe Gautier⁴, Elena Marchisella⁵, Neil R. Hardingham⁶, Robert A. Chesters⁷, Helen
948 Torrance¹, David M. Howard^{8,9}, Maurits A. Jansen¹⁰, Melanie McMillan¹¹, Yasmin Singh¹²,
949 Michel Didier¹³, Frank Koopmans², Colin A. Semple⁴, Andrew M. McIntosh⁹, Hansjürgen
950 Volkmer¹⁴, Maarten Loos⁵, Kevin Fox⁶, Giles E. Hardingham³, Anthony C. Vernon^{7, 15}, David
951 J. Porteous¹, August B. Smit², David J. Price³, J. Kirsty Millar^{1*}

952

953 ¹Centre for Genomic and Experimental Medicine, MRC Institute of Genetics and Molecular
954 Medicine at the University of Edinburgh, Edinburgh, UK

955 ²Department of Molecular and Cellular Neurobiology, Center for Neurogenomics and
956 Cognitive Research, VU University, Amsterdam, The Netherlands

957 ³Centre for Discovery Brain Sciences, Hugh Robson Building, The University of Edinburgh,
958 Edinburgh, UK

959 ⁴MRC Human Genetics Unit, MRC Institute of Genetics and Molecular Medicine at the
960 University of Edinburgh, Edinburgh, UK

961 ⁵Sylics Synaptologics BV, Amsterdam, The Netherlands

962 ⁶School of Biosciences, Museum Avenue, Cardiff University, Cardiff, UK

963 ⁷Department of Basic and Clinical Neuroscience, Institute of Psychiatry, Psychology and
964 Neuroscience, King's College London, London, UK

965 ⁸Social, Genetic and Developmental Psychiatry Centre, Institute of Psychiatry, Psychology &
966 Neuroscience, King's College London, UK

967 ⁹Division of Psychiatry, Kennedy Tower, The University of Edinburgh, Edinburgh, UK

968 ¹⁰Edinburgh Preclinical Imaging, The Chancellor's Building, The University of Edinburgh,
969 Edinburgh, UK,
970 ¹¹Centre for Reproductive Health, The Queen's Medical Research Institute, The University of
971 Edinburgh, Edinburgh, UK
972 ¹²Centre for Genomics and Transcriptomics, Paul-Ehrlich-Straße 23, D-72076, Tübingen,
973 Germany
974 ¹³Translational Sciences at Sanofi, Chilly-Mazarin, France
975 ¹⁴Department of Molecular Biology, NMI Natural and Medical Sciences Institute at the
976 University of Tübingen, Reutlingen, Germany
977 ¹⁵MRC Centre for Neurodevelopmental Disorders, King's College London, London, UK
978
979 *Corresponding author
980 Tel: +44 (0)131 651 8732
981 Fax: +44 (0)131 651 1059
982 Email: kirsty.millar@igmm.ed.ac.uk
983 [Address: Centre for Genomic and Experimental Medicine](#), MRC Institute of Genetics and
984 Molecular Medicine at the University of Edinburgh, Crewe Road, Edinburgh, EH4 2XU, UK
985
986

987 **Materials and methods**

988 **Mouse colony maintenance**

989 Mice were housed in the Biomedical Research Facility at the University of Edinburgh. All
990 mice were maintained in accordance with Home Office regulations, and all protocols were
991 approved by the local ethics committee of the University of Edinburgh. Mouse genotyping
992 was carried out as previously described¹.

993

994 **Perfusion fixation and brain isolation**

995 Mice were anaesthetized with intraperitoneal injection of 0.1ml/10g Fentanyl/Fluanisone
996 (Hypnorm®) and Midazolam (Hyponovel®). Deep anaesthesia was ensured by measuring
997 withdrawal reflexes. The mice were then transcardially perfused with 4% paraformaldehyde
998 at a rate of 0.2-0.5 ml/second. Brains were dissected out and the olfactory bulbs and
999 cerebellum removed. Brains were transferred to 4% neutral buffered formalin for 24 hr, then
1000 stored in 70% ethanol.

1001

1002 **Magnetic resonance imaging**

1003 Brains were taken from twelve same-sex littermate genotype trios (one wild-type, one
1004 heterozygote, one homozygote from the same litter, six male and six female trios). Brains
1005 were removed from 70% ethanol and incubated for three weeks in 8mM gadolinium contrast
1006 agent. Brains were then transferred to a 2ml Eppendorf tube filled with Fomblin and scanned
1007 in pairs using a three-dimensional gradient echo pulse sequence and an Agilent 7T
1008 DirectDrive MRI scanner, with acquisition parameters as follows; matrix 512x192x192
1009 (reconstructed to 512x256x256); field of view 40x10x10 mm; repetition time/echo time
1010 (TR/TE) 30/10 ms; 20 signal averages; total scan time 8.2 hours. A 26mm radiofrequency
1011 coil was used for signal transmission and reception. Magnetic resonance images were
1012 processed blind to genotype using a combination of FSL², ANTs³ and in-house C++ software
1013 utilizing the ITK library, available from <https://github.com/spinacist/QUIT>^{4, 5}. In brief, multi-

1014 head scans were bias-field corrected⁶ before being split into individual sample images.
1015 Registration was then performed between each subject and the Dorr atlas image⁷ to ensure
1016 all samples were aligned. An average study template image was then constructed using MR
1017 images from all animals⁸. The resulting template was then non-linearly registered to the atlas
1018 image. All subject images were then non-linearly registered to the study template. The
1019 inverse transforms from the atlas to the study template and from the study template to each
1020 subject were applied to calculate the total brain volume and individual brain region of interest
1021 (ROI) volumes of each subject. ROIs match those found in the Dorr atlas⁷.

1022

1023 **Histology**

1024 Five 9 week old male littermate genotype trios were used for histological analysis except
1025 where indicated below. Perfused brains were removed from 70% ethanol and paraffin wax-
1026 embedded, then sections were cut from three different zones of the brain; Bregma \approx 2.46
1027 (prefrontal cortex); Bregma \approx 0.75 (lateral ventricles and corpus callosum); Bregma \approx -1.94
1028 (hippocampus). Brains were processed by the University of Edinburgh Shared University
1029 Research Facilities (SURF), using a Leica RM2235 base sledge microtome. Twenty coronal
1030 sections of 10 μ m were cut for each block. Sections were mounted on to Superfrost Plus
1031 slides (ThermoFisher Scientific) and oven-dried. Two successive sections were used per
1032 location for each procedure.

1033 To visualize cytoarchitecture by Nissl staining, sections were dewaxed in xylene,
1034 then rehydrated through graded alcohols. Rehydrated slides were incubated for 2 minutes in
1035 0.2 % Cresyl fast violet solution containing 10 drops of acetic acid per 100 ml. Sections were
1036 dehydrated through graded alcohols, then cleared in xylene and cover-slipped with the
1037 xylene-based mounting solution DPX (Fisher Scientific).

1038 To examine Parvalbumin-expressing neurons, sections were dewaxed and
1039 endogenous peroxidase activity quenched by incubating in methanol containing 1%
1040 hydrogen peroxide for 30 minutes. Sections were incubated in 10 mM sodium citrate buffer

1041 at room temperature, then microwaved for 20 minutes at high power. Sections were cooled
1042 on ice for 20 minutes, then blocked using 20% normal goat serum (Vector) for 1 hour.
1043 Sections were next incubated overnight at 4°C with mouse anti-Parvalbumin primary
1044 antibody (Sigma-Aldrich P3088, 1:400 dilution), followed by incubation at room temperature
1045 for one hour with biotinylated goat anti-mouse secondary antibody (Sigma-Aldrich, 1:200
1046 dilution). Next, sections were incubated in Vectastain Elite Avidin-Biotin Complex (Vector
1047 Laboratories) for 30 minutes before visualization by incubation with 0.05% 3,3'-
1048 diaminobenzidine tetrahydrochloride (DAB, Sigma-Aldrich) containing 0.001% hydrogen
1049 peroxide. Finally, sections were dehydrated through graded alcohol, cleared in xylene, and
1050 cover slipped with DPX. To analyse the distribution of interneurons, the prefrontal cortex
1051 sections were initially separated into different regions of interest, distinguished using
1052 anatomical features and the Mouse Brain Atlas in stereotaxic coordinates⁹, then combined.
1053 In the hippocampal sections interneurons were counted in CA1 and the dentate gyrus, as
1054 well as the whole hippocampal area. ROIs were set at the same position on each section and
1055 the cells were counted manually, blind to genotype, using the Fiji 'Cell Counter' plugin.

1056 To examine apoptotic cells, the same procedure was used except the primary
1057 antibody was specific for active (cleaved) caspase-3 (Sigma-Aldrich, AB3623, 1:70 dilution),
1058 the secondary antibody was biotinylated goat anti-rabbit (Sigma-Aldrich, 1:200 dilution), with
1059 nickel was added to the DAB solution. Sections were counterstained with Nuclear Fast Red
1060 (Vector Laboratories).

1061 For cortical layer measurements in barrel cortex, brains were taken from three to five
1062 month old mice and immediately placed in 4% paraformaldehyde overnight. Fixed brains
1063 were sectioned using a cryostat (Leica) coronally at 50µm from rostral to caudal. Sections
1064 were mounted onto Superfrost slides (VWR) in gelatin solution. The slices were washed in
1065 acetone and water, then stained in 1% thionin-Nissl and dehydrated in increasing
1066 concentrations of alcohol, cleared in xylene and then coverslipped using DPX (Fluka).

1067

1068 **Image analysis**

1069 For most purposes, images of brain sections were captured using a dotSlide scanner
1070 (Olympus). Equivalent areas of both hemispheres were quantified on each slide, blind to
1071 genotype, then averaged per animal. Cell density was determined within the regions of
1072 interest shown (Supplementary Figure 2), which were manually drawn and set using the Fiji
1073 region of interest manager, with area determined and cells counted using the Fiji 'Cell
1074 Counter' plugin.

1075 For cortical layer measurements in barrel cortex, brain sections were imaged using a
1076 light microscope (Olympus). Barrel cortex could be identified by the presence of barrels in
1077 layer IV cortex (Bregma anterior-posterior 0.38 to -1.94mm) whilst sections of brain
1078 containing prefrontal cortex (Bregma 2.80 to 2.10mm) were identified using a mouse brain
1079 atlas⁹. Analysis of cortical thickness was performed within distinct brain areas. For cortical
1080 layer thickness, layers I, II/III, IV and V/IV were measured as distances perpendicular to the
1081 pial surface in addition to the total cortical thickness in barrel cortex. Total cortical thickness
1082 between the central sulcus and white matter for limbic cortex was measured for prefrontal
1083 cortex using Camera Lucida (Olympus).

1084

1085 **RNA sequencing**

1086 Hippocampi, and cortices minus hippocampus, cerebellum and olfactory bulbs, were
1087 dissected from the right brain hemisphere mice at nine weeks of age. Samples were snap
1088 frozen in liquid nitrogen and stored at -80°C, then processed in batches of mixed genotypes
1089 to extract the RNA. Total RNA samples were assessed with a Fragment Analyser (Agilent)
1090 for quality and integrity of total RNA. Libraries were prepared using 100ng of each total RNA
1091 sample using the TruSeq Stranded mRNA Library Prep Kit (Illumina). Single end RNA
1092 Sequencing was carried out to a depth of approximately 60 to more than 100 million reads.
1093 Demultiplexing of sequencing reads was carried out using CASAVA (version 1.8.2, Illumina),
1094 with adapters trimmed using Skewer (version 0.1.116)¹⁰. Raw sequence reads were mapped
1095 to mouse reference genome mm10 using STAR (version 2.4.0h)¹¹.

1096 Raw counts at gene level were obtained using htseq-count¹² (version 0.7.2, in the
1097 default union mode) on the alignment bam files and the Ensembl release 85 mouse gtf file.
1098 Differential gene expression was analysed using DESeq2 from the R statistical
1099 package¹³. Differential exon expression was analysed using DEXSeq¹⁴ (version
1100 1.19.4) using exon counts obtained by running the script “dexseq_count.py” provided
1101 by the Deseq package. Adjusted-p-values were calculated via a Benjamini-Hochberg
1102 Procedure to get False Discovery Rate (FDR), the default in Deseq2 package. Raw
1103 count data for all samples were together subjected to a regularised logarithm
1104 transformation¹⁰ using the DESeq2 package version 1.16.1. For each heat map, the
1105 transformed counts for each gene were normalised to Z-scores across all samples.
1106 Heat maps of gene expression were generated using R (version 3.4.2) and RStudio
1107 (version 1.0.143).

1108

1109 **Expression-weighted cell-type enrichment (EWCE) analysis**

1110 This analysis used the Karolinska Institute ‘Superset’ of RNASeq profiles generated from six
1111 independent single cell RNASeq studies of several brain regions and cell types. The
1112 Superset consists of 24 cellular classes generated by hierarchical clustering of nearly 9,970
1113 mouse brain single cell RNASeq profiles (all generated by exactly the same method)
1114 followed by cell type identity assignment¹⁵. Profiles consist of a set of specificity values
1115 which provide a measure of gene expression enrichment (calculated from mean expression
1116 of each gene in a cellular class divided by its mean expression in all cellular classes) for
1117 each gene detected in that class¹⁵. Some cells were isolated from mouse cortex,
1118 hippocampus, striatum, hypothalamus and midbrain, while others were the result of
1119 specifically isolating cortical Parvalbumin-positive interneurons or oligodendrocytes from
1120 multiple brain regions including somatosensory cortex and hippocampus. The ages of the
1121 mice used to generate the profiles include embryonic and a range from P14 to P90. Each
1122 class and profile is therefore an amalgamation of single cell profiles from closely related cell

1123 types, not all necessarily from the same brain region or age. Superset profiles were
1124 downloaded from http://hjerling-leffler-lab.org/data/scz_singlecell using specificity table:
1125 `ctd[[1]]$specificity` and expression table: `ctd[[1]]$mean_exp`. Analysis was carried out in the
1126 R package using script downloaded from <https://github.com/NathanSkene/EWCE/> ([version](#)
1127 [0.99.2](#)), and default options with Bonferroni multiple testing correction. The full list of
1128 [expressed *Der1* cortex or hippocampus genes was used as background, as appropriate](#). The
1129 script was run with 10,000 repetitions. The Superset samples were sequenced at a lower
1130 depth than the *Der1* samples, and using unique molecular identifiers. Consequently only the
1131 most abundantly expressed genes (up to 14,581) were detected. For cortex, 1,794 of 2,125
1132 dysregulated genes are present in the Superset profiles. For hippocampus, 151 of 175
1133 dysregulated genes are present in the Superset profiles. *Der1* whole gene DESeq2 RNASeq
1134 data were used for this analysis.

1135

1136 **RNASeq deconvolution**

1137 RNASeq deconvolution was carried out using the cell Karolinska Institute 'Superset' of
1138 RNASeq profiles¹⁵ described above under EWCE analysis as reference. Specificity value
1139 thresholds of 0.75 and 0.6 were set to ensure that the most highly enriched genes were used
1140 in this analysis, thus profile signatures consisted of genes with at least one specificity value
1141 in one cell type above these thresholds. To provide context, specificity value=1 represents
1142 100% specificity for one cell class, the astrocyte marker *Gfap* exhibits a specificity value of
1143 0.87 in the astrocyte/ependymocyte class, the oligodendrocyte marker *Mbp* exhibits a
1144 specificity value of 0.6 in the oligodendrocyte class, the interneuron marker *Parvalbumin*
1145 exhibits specificity values of 0.41 and 0.27 in the interneuron and striatal interneuron
1146 classes, respectively, and the synapse marker *Dlg4* (*Psd95*) exhibits specificity values of
1147 ~0.1 in pyramidal neurons and <0.1 in other neuron classes¹⁵. This resulted in the use of 346
1148 genes for threshold=0.75, and 752 genes for threshold=0.6, of which 285 and 653 are
1149 present in our wild-type RNASeq data.

1150 Deconvolution was carried out using CIBERSORT Jar Version 1.06 (May 5th 2017)¹⁶,
1151 available at the web interface <https://cibersort.stanford.edu>. The ability of CIBERSORT to
1152 accurately deconvolute the 24 cell types in the Superset was examined by creating artificial
1153 cell mixes by combining Superset gene expression values in various proportions from 0 to
1154 0.5. CIBERSORT input was then compared to output to determine the efficiency of artificial
1155 sample deconvolution for the 24 cell types.

1156

1157 **Pathway analysis**

1158 DESeq2 data were examined separately or combined with DEXSeq data by Ingenuity
1159 Pathway Analysis (IPA, Qiagen), using corrected p values and log2 fold changes, and the
1160 corresponding full list of expressed genes for each brain region as the background gene set.
1161 Human t(1;11) translocation neuron RNASeq data¹ were similarly analysed using IPA.
1162 Pathway analysis of putative schizophrenia or depression risk genes was carried out using
1163 IPA and the full cortical gene expression list as the background gene set. Pathway analysis
1164 of dysregulated orthologues of putative schizophrenia or depression risk genes used the
1165 corresponding full list of expressed genes for each brain region as the background set.
1166 Adjusted $p < 0.05$, and $z > 2$ or $z < -2$ were used as thresholds throughout. Pathway analysis of
1167 dysregulated genes from cell class profiles used the full Superset profile as background. A
1168 specificity value threshold of 0.2 was set to ensure that a sufficient number of the most
1169 specific genes were used in the analysis. For context regarding specificity values see
1170 deconvolution, above. Where DEXSeq identified dysregulated sequences that did not
1171 unambiguously map to a single gene, or mass spectrometry identified peptides that could
1172 not be unambiguously mapped to a single protein (due to close homology with other
1173 proteins), all possible genes and proteins were included in the pathway analysis.

1174

1175 **Synaptosome preparation and mass spectrometry**

1176 Synaptosomes were prepared from 8-10 week old *Der1* cortex and hippocampus (six wild-
1177 type, five heterozygous, five homozygous) as previously described¹⁷. Tissue was

1178 homogenized in HEPES buffer (5 mM HEPES, pH 7.4, 0.32 M sucrose supplemented with
1179 protease inhibitor cocktail, Roche) and centrifuged at 1000 x g for 10 min at 4°C. The
1180 supernatant was subsequently centrifuged in a 0.85/1.2 M sucrose gradient at 100,000 x g
1181 for 2 hours. Synaptosomes were recovered from the 0.85/1.2 M sucrose interface and
1182 concentrated by centrifugation at 18,000 x g for 30 min.

1183 Samples were digested using filter aided sample preparation (FASP) with some
1184 modifications¹⁸. Briefly, 20 µg of each protein sample were incubated with 75 µL 2% SDS, 1
1185 mM Tris(2-carboxyethyl)phosphine at 55°C for 1 hour, after which samples were incubated
1186 with 0.5 µL 200 mM methyl methanethiosulfonate for 15 min. Next, 200 µL 8 M Urea in Tris
1187 pH 8.8 were added and the samples were transferred to Microcon-30 filter tubes (Millipore).
1188 Samples were washed 4 times with 8M Urea in Tris buffer and 4 times with 50 mM
1189 ammonium bicarbonate by centrifugation at 14,000 x g for 10 min each. Proteins were
1190 digested with 0.7 µg Trypsin/Lys-C Mix (MS grade, Promega) overnight at 37°C. Peptides
1191 were eluted with 200 µL 50 mM ammonium bicarbonate, dried in SpeedVac and stored at -
1192 20°C.

1193 Peptides were analysed by micro LC MS/MS using an Ultimate 3000 LC system
1194 (Dionex, Thermo Scientific) and the TripleTOF 5600 mass spectrometer (Sciex). Peptides
1195 were trapped on a 5 mm Pepmap 100 C18 column (300µm i.d., 5µm particle size, Dionex)
1196 and fractionated on a 200 mm AlltimaC18 column (300µm i.d., 3µm particle size). The
1197 concentration of acetonitrile in the mobile phase was increased at a flow rate of 5µL/min
1198 from 5 to 18% in 88 min, to 25% at 98 min, 40% at 108 min and to 90% in 2 min. Peptides
1199 were electro-sprayed into the mass spectrometer with a micro-spray needle (at 5500 V). The
1200 mass spectrometer was operated in a data-independent mode, as described in¹⁹. Each cycle
1201 consisted of a parent ion scan of 150 msec and 8 Da MS/MS windows (80 msec scan time
1202 each), throughout a 450-770 m/z mass range. The collision energy for each window was
1203 calculated for a 2+ ion centered upon the window (spread of 15 eV).

1204 The data were analysed with Spectronaut Pulsar v 12.0.20491.21.28109²⁰ and using
1205 a spectral library created by data-dependent acquisition from hippocampal synapse-enriched

1206 samples containing spike-in iRT peptides (Biognosys). Cross-run normalization was enabled
1207 using local normalization strategy. Only peptides quantified with a Q-value $\leq 10^{-2}$ and 10^{-3}
1208 (for hippocampus and cortex datasets, respectively) across all samples in at least two
1209 groups were considered. Limma R package was used to Loess normalize protein abundance
1210 ('normalizeCyclicLoess' function, 'fast' method and 10 iterations). Volcano plots were
1211 generated using R (version 3.6.2). Protein were annotated to synaptic genes and sunburst
1212 plots were generated using SynGO 1.0 database and online tool²¹.

1213

1214 **Hippocampal Cell Culture and Electrophysiological recordings**

1215 Primary hippocampal cultures were prepared from individual E17.5 DER littermate pups as
1216 described²². Briefly, hippocampi were dissected from pups, incubated in Papain, dissociated
1217 and grown in Neurobasal A growth medium containing 1% Rat Serum and supplemented
1218 with B-27, and maintained until Days In Vitro (DIV) 21.

1219 Whole cell patch clamp recordings were performed as described²³. Briefly,
1220 coverslips containing DIV 21 hippocampal neurons were transferred to a recording chamber
1221 with a constant (3-5ml/min) perfusion of external recording solution containing: 150 mM
1222 NaCl, 2.8 mM KCl, 10 mM HEPES, 2 mM CaCl₂, 10 mM D-glucose and 100 μ M glycine, pH
1223 7.35, 320 mOsm. Tetrodotoxin citrate (300 nM) was included to block action-potential driven
1224 excitatory events. Patch-pipettes were pulled from borosilicate glass (Harvard Apparatus,
1225 Kent, UK) with a resistance of 3-5 M Ω , and filled with a K-gluconate-based internal solution
1226 containing: 141 mM Potassium Gluconate, 2.5 mM NaCl, 10 mM HEPES, 11 mM EGTA, pH
1227 7.35). Currents were evoked by S-AMPA (50 μ M) and NMDA (150 μ M). All currents were
1228 recorded at room temperature, using an axopatch 200B amplifier (Molecular Devices, Union
1229 City, CA). Neurons were voltage-clamped at -60 mV. Whole-cell currents were analysed
1230 using WinEDR v3.2 software (John Dempster, University of Strathclyde, UK), with currents
1231 normalised to cell capacitance. For statistical analysis, n was taken as the number of pups,
1232 with n=3 WT, 4 HET and 3 HOM. A total of 12 WT, 14 HET and 11 HOM genotype
1233 coverslips were recorded from.

1234

1235 **Statistical analysis**

1236 For analysis of MRI data, a multivariate general linear model 2-way MANCOVA statistical
1237 test was performed using SPSS statistics 22 (IBM) to determine group-level differences in
1238 brain ROI volumes with genotype as fixed effect, total brain volume and brain region as
1239 dependent variable, and littermate trio groupings as covariate.

1240 For enrichment analysis, hypergeometric probabilities were calculated using
1241 keisan.casio.com/exec/system/1180573201. As with the pathway analysis, where DEXSeq
1242 identified dysregulated sequences that did not unambiguously map to a single gene, or mass
1243 spectrometry identified peptides that could not be unambiguously mapped to a single protein
1244 (due to close homology with other proteins), all possible genes and proteins were included in
1245 the enrichment analysis.

1246 For the proteomic analysis, empirical Bayes moderated t-statistics with multiple
1247 testing correction by false discovery rate were performed on log-transformed protein
1248 abundances ('eBayes' and 'topTable' functions from Limma R package), as previously
1249 described^{18, 19, 24, 25}. Proteins with a FDR adjusted p-value < 0.05 were considered
1250 significantly regulated for subsequent downstream analysis.

1251 Other statistical analyses were carried out using GraphPad Prism, with statistical
1252 tests used stated in figure legends.

1253

1254 **Supplementary Table 1** (Excel file) Magnetic resonance imaging data. Both hemispheres,
1255 regional volumes (mm³) corrected to individual whole brain volumes, left and right
1256 hemispheres combined, separate hemispheres, regional volumes (mm³) corrected to
1257 individual whole brain volumes, left and right hemispheres considered separately

1258

1259 **Supplementary Table 2** (Excel file) RNA sequencing data. **a** DeSeq2 (whole gene
1260 differential expression) *Der1* cortex data, **b** DEXSeq (exon level differential expression) *Der1*

1261 cortex data, **c** DeSeq2 (whole gene differential expression) *Der1* hippocampus data, **d**
1262 DEXSeq (exon level differential expression) *Der1* hippocampus data. In each case data are
1263 provided with comparisons to human iPSC-derived cortical neuron cultures from members of
1264 the t(1;11) family¹², two large-scale genome-wide association studies of schizophrenia^{1, 2},
1265 synapse genes from a large-scale schizophrenia CNV study³, two large-scale genome-wide
1266 association studies of depression^{4, 6}, a large-scale genome-wide association study of bipolar
1267 disorder⁵, a large-scale genome-wide association study of Alzheimer's Disease⁵⁵ where
1268 matches were found, and a large-scale genome-wide association study of cerebral cortex
1269 architecture⁶⁵, where matches were found (references numbered according to main text).
1270 Overlaps are represented by a gene name in the relevant genetic study column. Non-
1271 overlaps are represented by empty cells, BaseMean, mean of normalised counts of all
1272 samples; p value, p value for wild-type versus heterozygous; adjusted p value, p value
1273 adjusted for multiple testing

1274

1275 **Supplementary Table 3** (Excel file) Dysregulated genes with conserved cAMP response
1276 elements according to <http://natural.salk.edu/creb/>.

1277

1278 **Supplementary Table 4** (Excel file) Ingenuity Pathway Analysis functions. **a** functions
1279 enriched for dysregulated genes in *Der1* cortex. All functions in the categories 'Molecular
1280 and cellular function' and 'Physiological system development and function' are included.
1281 Selected top relevant functions are provided in Table 1. Data are provided with comparisons
1282 to functions predicted from human iPSC-derived cortical neuron cultures from members of
1283 the t(1;11) family¹² (reference numbered according to main text). Overlaps are represented
1284 by an x in the human neuron column. Non-overlaps are represented by empty cells, **b**,
1285 functions enriched for dysregulated genes in *Der1* hippocampus. All functions in the
1286 categories 'Molecular and cellular function' and 'Physiological system development and
1287 function' are included. Selected top relevant functions are provided in Supplementary Table

1288 5. **c**, functions enriched for dysregulated genes in Superset cell classes. All functions in the
1289 categories 'Molecular and cellular function' and 'Physiological system development and
1290 function' are included. Selected top relevant functions are provided in Supplementary Table
1291 6. **d**, functions enriched for dysregulated genes in human iPSC-derived cortical neuron
1292 cultures from members of the t(1;11) family. All functions in the categories 'Molecular and
1293 cellular function' and 'Physiological system development and function' are included. Selected
1294 top relevant functions are provided in Table 1. The genes listed for each function are
1295 dysregulated in the corresponding dataset.
1296

1297 **Supplementary Table 5** Top predicted relevant altered functions in heterozygous *Der1*
 1298 mouse hippocampus.

Function (no. of molecules ^a)	<i>Der1</i> hippocampus score (no. of genes ^b)
General cell morphology	
Development of neurons (1,423)	p=2e-9 (33)
Morphology of neurons (1,123)	p=8e-7 (22)
Maturation of neurons (114)	p=8e-6 (7)
Abnormal morphology of neurons (923)	p=3e-5 (16)
Differentiation of neurons (648)	p=5e-4 (14)
Cell contact	
Adhesion of neuronal cells (89)	p=8e-9 (9)
Formation of plasma membrane (406)	p=1e-8 (17)
Cell-cell contact (1,118)	p=1e-5 (22)
Cell-cell contact of neurons (24)	p=1e-5 (4)
Cell-cell adhesion of neurons (22)	p=3e-4 (3)
Cytoskeleton	
Microtubule dynamics (2,247)	p=2e-4 (31)
Organization of cytoskeleton (2,624)	p=7e-4 (33)
Cellular protrusions/neurites	
Neuritogenesis (1,067)	p=2e-6 (23)
Formation of cellular protrusions (1,645)	p=1e-4 (26)
Growth of neurites (910)	p=2e-4 (16)
Branching of cells (746)	p=2e-4 (14)
Extension of neurites (267)	p=5e-4 (8)
Axons	
Extension of axons (134)	p=5e-3 (5)
Myelination of optic nerve (8)	p=2e-3 (2)
Myelination (8)	p=5e-3 (7)
Dendrites	
Formation of dendrites (209)	p=2e-4 (8)
Dendritic growth/branching (446)	p=4e-4 (10)
Density of dendritic spines (143)	p=1e-3 (5)
Morphology of dendrites (138)	p=3e-3 (5)
Length of dendrites (47)	p=3e-3 (3)
Cell proliferation	
Proliferation of epithelial cells (996)	p=3e-3 (14)
Neurogenesis of cerebral cortex (69)	p=5e-3 (3)
Proliferation of stem cells (372)	p=8e-3 (7)
Transport	
Exocytosis (336)	p=9e-4 (8)
Transport of dopamine (76)	p=8e-4 (3)
Secretion of neurotransmitter (248)	p=1e-3 (7)
Release of neurotransmitter (510)	p=1e-3 (7)
Transport of 5-hydroxytryptamine (40)	p=2e-3 (2)
Neurotransmission	
Developmental process of synapse (303)	p=3e-9 (16)
Neurotransmission (716)	p=8e-8 (20)
Synaptic transmission (558)	p=3e-7 (17)
Maturation of synapse (36)	p=3e-5 (4)
Miniature excitatory postsynaptic currents (71)	p=2e-4 (5)
Plasticity of synapse (170)	p=3e-4 (7)
Excitatory postsynaptic potential (166)	P=3e-4 (7)
Paired-pulse facilitation of synapse (55)	p=9e-4 (4)
Action potential of cells (238)	p=1e-3 (7)
Formation of excitatory synapses (14)	p=3e-3 (2)

1299
 1300 A full list of functions is provided in Supplementary Table 4b. Related functions are grouped,
 1301 with top functions shown for each group. a, total number of molecules relating to each IPA
 1302 function; b, number of dysregulated genes relating to each function
 1303

1304 **Supplementary Table 6** Top predicted relevant altered cellular functions in cell classes from
 1305 EWCE analysis.

Superset cell class	
Function (no. of molecules^a)	<i>Der1</i> cortex score (no. of genes^b)
<i>Der1</i> cortex pyramidal CA1	
Long-term potentiation (539)	p=6e-6 (8)
Neurotransmission (773)	p=5e-5 (9)
Excitation of cerebral cortex cells (46)	p=6e-5 (3)
Synaptic transmission (601)	p=6e-5 (8)
Excitation of neurons (167)	p=9e-5 (4)
Remodelling of F-actin structure (7)	p=1e-4 (2)
Development of neurons (1,474)	p=2e-4 (12)
Neuritogenesis (1,110)	p=3e-4 (10)
AMPA mediated synaptic current (9)	p=3e-4 (2)
Activation of neurons (252)	p=3e-4 (4)
<i>Der1</i> cortex pyramidal somatosensory	
Efflux of dopamine (63)	p=2e-5 (3)
Quantity of dense core vesicles	p=2e-4 (2)
Neurotransmission (773)	p=3e-4 (9)
Synaptic transmission 601)	p=3e-4 (8)
Exocytosis by eukaryotic cells (99)	p=1e-3 (3)
Fusion of synaptic vesicles (21)	p=1e-3 (2)
Action potential of neurons (198)	p=3e-3 (4)
Quantity of synapse (92)	p=3e-3 (3)
Accumulation of cortical actin filaments (1)	p=4e-3 (1)
Activation of parvocellular neurons (1)	p=4e-3 (1)
<i>Der1</i> cortex interneurons	
Neurotransmission (773)	p=7e-6 (7)
Activation of neurons (252)	p=1e-5 (4)
Action potential of neurons (198)	p=5e-5 (4)
Excitation of neurons (167)	p=2e-4 (3)
GABA-mediated receptor currents (14)	p=2e-4 (2)
Fusion of plasma membrane (34)	p=4e-4 (2)
Excitation of cerebral cortex cells (46)	p=5e-4 (2)
Activation of enzyme (584)	p=9e-4 (5)
Accumulation of 2-arachidonoylglycerol (3)	p=1e-3 (1)
Activation of parvocellular neurons (1)	p=1e-3 (1)
<i>Der1</i> cortex astrocytes/ependymocytes	
Fatty acid metabolism (1,492)	p=3e-8 (17)
Concentration of lipid (2,135)	p=3e-7 (19)
Uptake of amino acids (264)	p=8e-7 (6)
Uptake of glutamine family amino acid (133)	p=9e-7 (5)
Function of neuroglia (56)	p=2e-6 (5)
Mass of fat (24)	p=2e-6 (4)
Transport of amino acids (394)	p=3e-6 (7)
Concentration of fatty acid (721)	p=4e-6 (10)
Function of central nervous system (152)	p=4e-6 (6)
Function of oligodendrocytes (9)	p=5e-6 (3)

1306
 1307 A full list of functions is provided in Supplementary Table 5c, e. The most highly enriched
 1308 genes that are dysregulated in *Der1* cortex for each cell class were used for IPA analysis,
 1309 with specificity value cut-off=0.2 (SV=1 indicates 100% specificity, see methods for more
 1310 context). In many cell classes the relatively low number of genes above this threshold was

1311 insufficient for meaningful pathway analysis. **a**, total number of molecules relating to each
1312 IPA function; **b**, number of dysregulated genes relating to each function

1313

1314 **Supplementary Table 7** (Excel file) Synaptosome mass spectrometry data. **a**, Mass
1315 spectrometry analysis of cortex synaptosomes isolated from wild-type (WT), heterozygous
1316 (HET) or homozygous (HOM) *Der1* mice, **b**, Mass spectrometry analysis of hippocampus
1317 synaptosomes isolated from wild-type (WT), heterozygous (HET) or homozygous (HOM)
1318 *Der1* mice, **c**, SynGo annotations. SD, standard deviation

1319 **Supplementary table 8** Comparison between characteristics of the *Der1* mouse and
 1320 pertinent characteristics of mutant mice that are known or proposed to be relevant to the
 1321 t(1;11) translocation.

Mutant	Brain structure	Synapses & plasticity	Electrophysiology	Neuronal intracellular transport
<i>Der1</i>	<p>↑ hippocampal Parvalbumin-positive interneuron density</p> <p>altered oligodendrocyte-myelin function²⁶</p> <p>no gross structural changes</p>	<p>↑ surface/synaptic NMDA receptor expression in cultured hippocampal neurons¹</p> <p>altered PSD95 distribution indicative of an increased density of weaker synapses¹</p> <p>altered expression of genes involved in synapse formation, structure & function</p> <p>altered expression of genes critical for synaptic plasticity and long-term potentiation, including the CREB signalling pathway</p>	<p>↓ AMPA/NMDA ratio in cultured hippocampal neurons</p>	<p>↑ NMDA receptor motility¹</p> <p>altered expression of genes required for vesicle transport and exo/endocytosis</p>
humanised DISC1-Boymaw & Boymaw-DISC1²⁷	<p>endogenous mouse <i>Disc1</i> gene replaced with human <i>DISC1-Boymaw</i> or <i>Boymaw-DISC1</i> cDNA fusion transgenes (<i>Boymaw</i> is otherwise known as <i>DISC1FP1</i>) resulting in <i>Disc1</i> promoter-driven forced expression of putative chimeric proteins²⁸ (whose expression in t(1;11) carriers remains to be established¹)</p>	<p>↓ cortical expression of NMDA receptor subunit GluN1 and PSD95²⁷</p>		
Disc1Δ2-3²⁹	<p>↓ density of Parvalbumin-positive interneurons in many cortical areas³⁰, and in hippocampus³¹</p> <p>no gross structural changes²⁹</p>	<p>catecholaminergic network dysfunction³²</p> <p>↓ methamphetamine-induced dopamine release & ↑ dopamine receptor expression in nucleus accumbens³¹</p>	<p>↑ threshold for induction of long-term potentiation in hippocampus²⁹</p>	<p>↓ dendritic ITPR1 mRNA transport in cultured hippocampal neurons³³</p> <p>↓ synaptic vesicle exocytosis³⁴</p>
Disc1-LI³⁵	<p>deletion of exons 1-3 from endogenous mouse <i>Disc1</i> gene, abolishes full-length <i>Disc1</i> expression</p>		<p>altered parvalbumin-positive interneuron function³⁶</p>	
Disc1_{tr}³⁷	<p>↓ density of Parvalbumin-positive interneurons in hippocampus and medial prefrontal</p>	<p>↓ NMDA receptor GluN2A & GluN2B, ↑ GluN1 (trend) protein expression in hippocampus³⁸</p>	<p>↑ long-term potentiation in Schaffer collateral commissural pathway temporoammonic long-term potentiation</p>	

1-8) fused to green fluorescent protein, expressed from transgenic mouse bacterial artificial chromosome under control of <i>Disc1</i> promoter	cortex, and displacement in dorsolateral prefrontal cortex ³⁷ ↑ lateral ventricle volume ↓ cerebral cortex thickness partial agenesis of corpus callosum ³⁷		abolished ³⁹ altered hippocampus-prefrontal cortex connectivity & reduced neurotransmitter release probability in the glutamatergic hippocampal CA1–prefrontal cortex projection ³⁸	
hDISC1 ⁴⁰ C-terminally truncated DISC1 (exons 1-8) transgene under inducible control of CaMKII promoter	↓ density of Parvalbumin-positive cortical interneurons ⁴¹ ↑ lateral ventricle volume ⁴⁰ altered oligodendrocyte specification ^{42, 43}	↓ cortical dopamine ⁴¹ & dopamine D2 receptor binding in olfactory tubercle and nucleus accumbens (trend) ⁴⁴ ↑ dendritic spine density ⁴¹ ↑ vesicular glutamate transporters in astrocytes ⁴⁵ ↑ NMDA receptor subunit GluN1, ↓ GluN2A in hippocampus ⁴⁵ altered homeostasis of dopamine and glutamate receptors in the nucleus accumbens ⁴⁶ reduced capacity of astrocytes to support dendritic and synaptic development ⁴⁷	↑ spontaneous excitatory postsynaptic currents in cultured cortical neurons ⁴⁸	altered expression of proteins required for vesicular transport ⁴⁹
DN-DISC1 ⁵⁰ C-terminally truncated DISC1 (exons 1-8) transgene under control of CamKII promoter	↓ density of Parvalbumin-positive cortical interneurons ⁵⁰ ↑ lateral ventricle volume ⁵⁰		oscillations in hippocampal CA1 ⁵¹ abnormal action potentials, and dopaminergic regulation, in fast spiking parvalbumin-positive interneurons of prefrontal cortex ⁵²	
DN-DISC1-PrP ⁵³ C-terminally truncated DISC1 (exons 1-8) transgene under control of PrP promoter	no gross structural changes ⁵³			
nes-DN-DISC1 ⁵⁴ C-terminally truncated DISC1 (exon 1-8) transgene inducibly expressed in neural precursor cells	↑ density of Parvalbumin-positive interneurons in cingulate cortex, retrosplenial granular cortex, and motor cortex ⁵⁴			
Disc1 ^{Tm1Kara 55} natural deletion within mouse <i>Disc1</i>	Parvalbumin-positive interneuron density unchanged ⁵⁶	↓ dendritic spine density & altered spine morphology in cultured hippocampal and	↓ short-term potentiation at hippocampal CA1-CA3 synapse	↓ synaptic vesicle volume at hippocampal CA3 synapses ⁵⁸

<p>exon 6 that introduces a premature termination codon, combined with targeted premature transcription termination signal in intron 8, abolishes full-length Disc1 expression and may express C-terminally truncated protein due to the termination codon within exon 7</p>	<p>↓ prefrontal cortex volume⁵⁶</p>	<p>cortical neurons⁵⁷ altered hippocampal CREB signalling⁵⁸</p>	<p>altered short-term plasticity at mossy fibre-CA3 circuit⁵⁸ ↑ neuronal excitability in medial prefrontal cortex⁵⁹ ↑ short-term depression & probable ↑ neurotransmitter release probability in medial prefrontal cortex⁵⁹ ↑ spontaneous excitatory postsynaptic currents in cultured cortical neurons⁴⁸ altered spontaneous inhibitory postsynaptic currents in cultured cortical neurons⁴⁸</p>	<p>proteomic changes suggest effects upon synaptic vesicle transport⁵⁹</p>
--	--	---	--	---

1322

1323 The mutants fall into three main categories 1) recapitulation of the gene fusion between
1324 *DISC1* and *DISCFP1* (*Der1*, transgenic *Boymaw* fusions), 2) elimination of full-length *Disc1*
1325 expression (*Der1*, transgenic *Boymaw* fusions, *Disc1*Δ2-3, DISC1-LI, *Disc1*^{Tm1Kara}), 3)
1326 transgenic overexpression of a truncated form of *Disc1* or *DISC1* encoded by exons 1-8 that
1327 was inferred to arise from the t(1;11) prior to discovery of the *DISC1/DISCFP1* gene fusion
1328 (*Disc1*_{tr}, h*Disc1*, DN-DISC1, DN-DISC1-PrP, nes-DN-DISC1).

THIS STUDY

Der1 mouse

endogenous *Disc1* allele modified to recapitulate effect of t(1;11) upon DISC1 expression

STRUCTURAL

whole brain imaging
magnetic resonance imaging to examine brain structure

Nissl staining of sections
to examine brain structure at the cellular level

OMICS

RNASeq analysis of tissue
to identify dysregulated genes

EWCE analysis of RNASeq data
to identify cellular classes targeted by the *Der1* mutation

gene specificity values for cell classes

RNASeq deconvolution of RNASeq data
to examine relative cell class proportions

expression data for genes with the highest specificity values in cell classes

pathway analysis
to identify molecular pathways impacted by the *Der1* mutation

comparison to t(1;11) human neuron cultures
to identify shared characteristics and confirm relevance of the *Der1* mouse to studies of the t(1;11)

mass spectrometry analysis of synaptosomes
to confirm synaptic changes

FUNCTIONAL

electrophysiology
to confirm altered synapse function

RELEVANCE TO MAJOR MENTAL ILLNESS

comparison between RNASeq and genetic data for major mental illness
to confirm relevance of the t(1;11) and *Der1* mouse

t(1;11) carriers

co-segregation of a balanced chromosomal translocation with major mental illness in a large family⁷⁻⁹

brain imaging
to identify structural & functional changes⁹⁻¹¹

linkage analysis
to establish statistical link between t(1;11) and major mental illness⁷⁻⁹

IPSC/neural cell derivation
to enable studies of live neural cells from t(1;11) carriers¹²

RNASeq analysis of neuron cultures
to identify dysregulated genes¹²

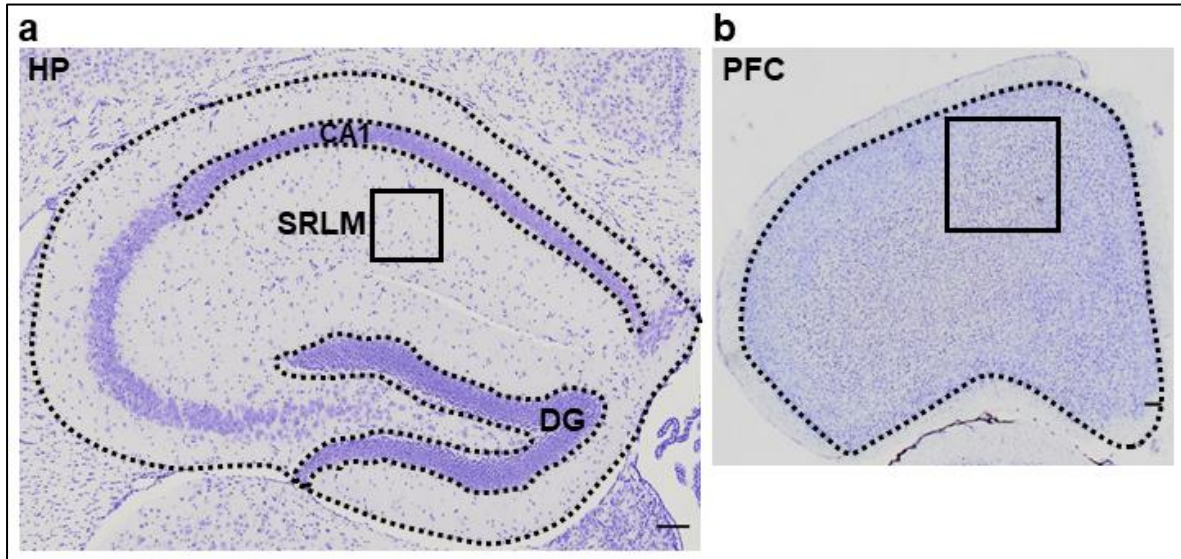
pathway analysis
to identify molecular pathways impacted by the t(1;11)

1330 **Supplementary Fig. 1** Flowchart indicating the experimental approach taken. Superscript
1331 numbers indicate references according to the main (not supplementary) text.
1332

1333

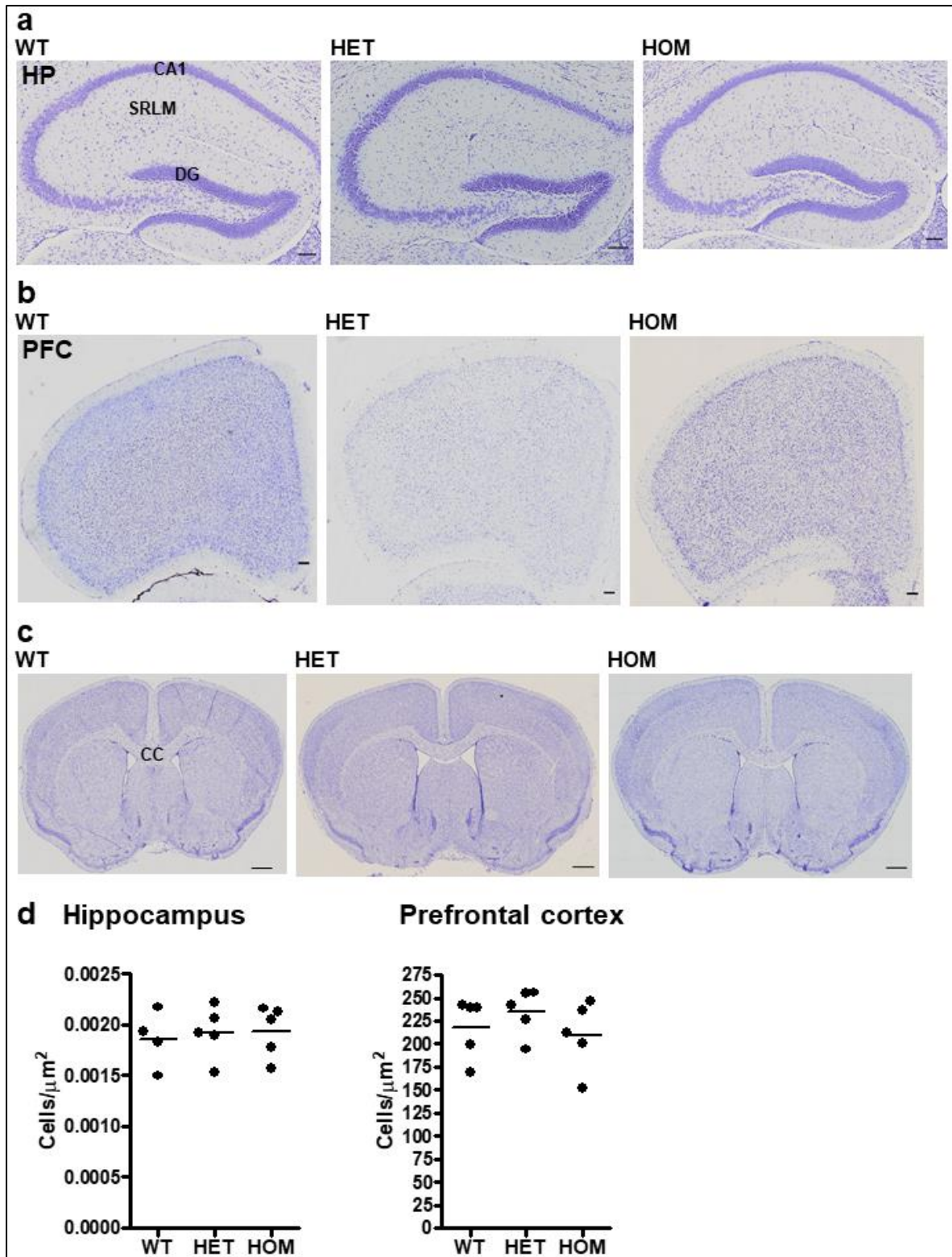
1334

1335



1336

1337 **Supplementary Fig. 2** Regions of interest for image analysis of cell density, Parvalbumin
1338 and cleaved Caspase 3. **a** Hippocampus (HP). The box indicates the region of the Stratum,
1339 Radiatum, Lacunosum and Moleculare (SRLM) in which cell density was quantified. Dotted
1340 lines outline the hippocampal formation, CA1 and the dentate gyrus (DG) used for
1341 quantification of Parvalbumin-positive cells and cells expressing cleaved Caspase 3. **b**
1342 Prefrontal cortex (PFC). The box indicates the region in which cell density was quantified.
1343 The dotted line outlines the region in which Parvalbumin-positive cells and cells expressing
1344 cleaved Caspase 3 were quantified. Scale bars, 100 μ m



1345

1346

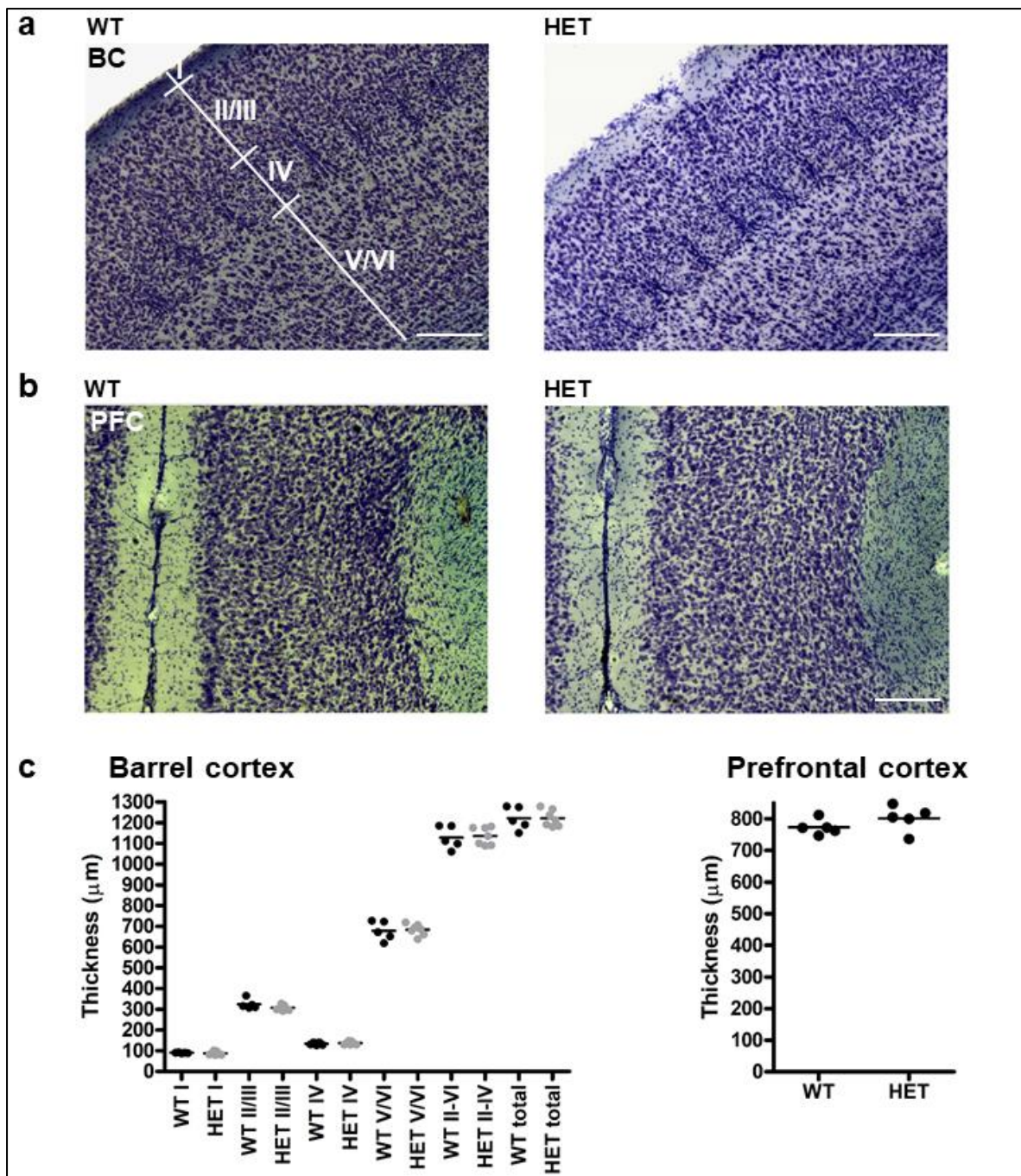
1347

1348

1349

Supplementary Fig. 3 Brain structure visualised by Nissl staining. Sections through hippocampus (HP) **a**, prefrontal cortex (PFC) **b**, and corpus callosum (CC) **c**, were stained with Nissl to visualise cell bodies and tissue structure. scale bars, 100 μm in **a** and **b**, 500 μm in **c** **d** Quantification of average cell density from both sides of the brain in hippocampal

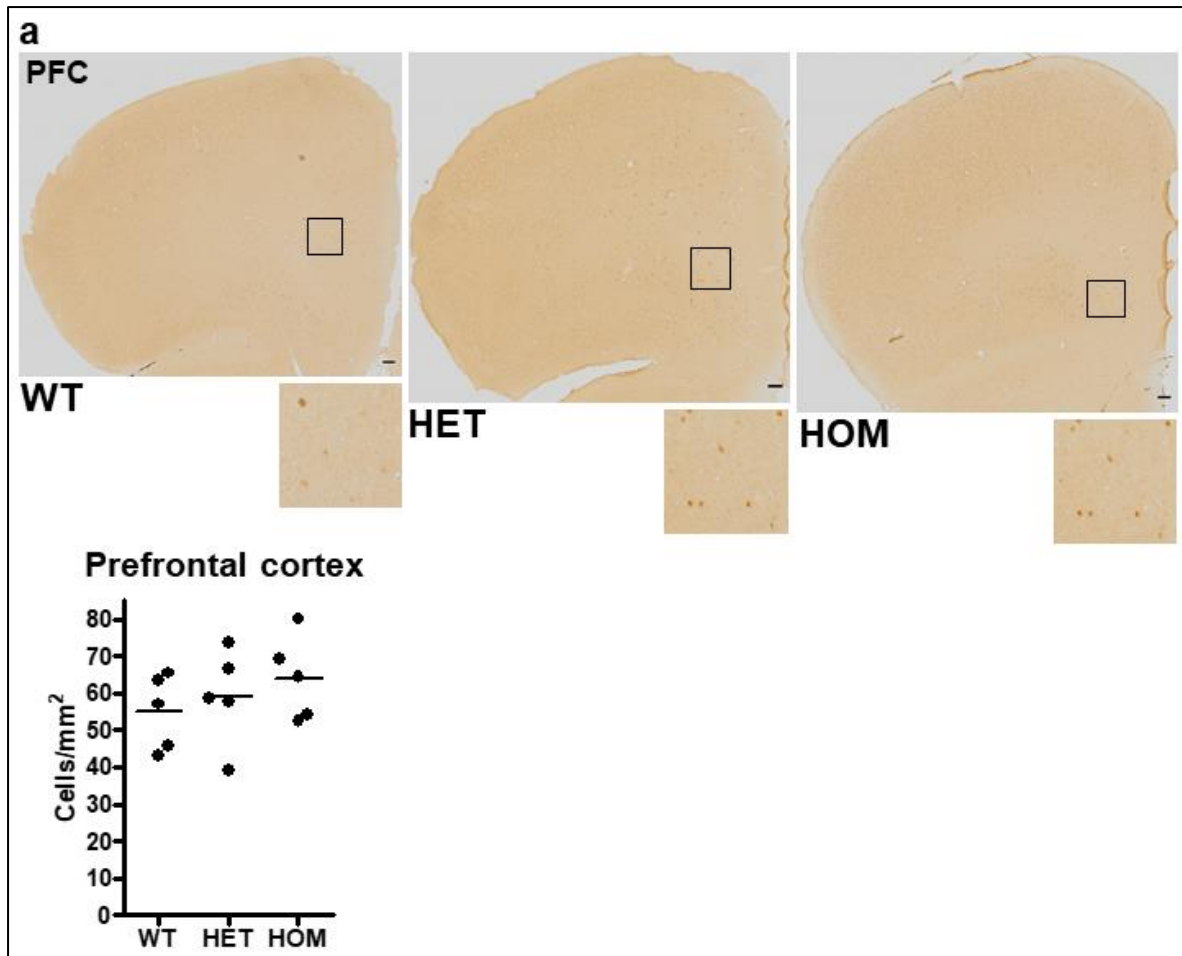
1350 Stratum, Radiatum, Lacunosum and Moleculare, and PFC. Data were analysed by Kruskal-
1351 Wallis one-way ANOVA. Horizontal line on graphs, average of values for each sample; WT,
1352 wild-type; HET, heterozygous *Der1*; HOM, homozygous *Der1*
1353



1354

1355 **Supplementary Fig. 4** Cortical layers visualised by Nissl staining. Barrel cortex was used to
 1356 examine layering in detail because the individual cortical layers could not be distinguished in
 1357 prefrontal cortex. Sections through barrel cortex (BC) **a**, and prefrontal cortex (PFC) **b**, were
 1358 stained with Nissl to visualise cell bodies and tissue structure. Cortical layers and
 1359 measurements taken are indicated. **c** Quantification of layer thickness in barrel cortex and
 1360 PFC. Two-way ANOVA found no effect of genotype on layer thickness ($F_{1,40}=0.1959$,
 1361 $p>0.05$), nor any interaction between layer thickness and genotype ($F_{3,40}=0.6631$, $p>0.05$) in

1362 barrel cortex. Unpaired two-tailed t-test found no effect of genotype on cortical thickness in
1363 PFC ($p=0.2$). Horizontal line on graphs, average of values for each sample; scale bars,
1364 200 μm ; WT, wild-type; HET, heterozygous *Der1*



1365

1366

Supplementary Fig. 5 No change in Parvalbumin-expressing interneuron density in *Der1*

1367

prefrontal cortex. **a** Prefrontal cortex (PFC) sections from nine week old mouse brain were

1368

stained with an antibody specific for Parvalbumin. Enlarged regions showing Parvalbumin-

1369

expressing interneurons are indicated by boxes. scale bars, 100 μ m **b** Average density of

1370

Parvalbumin-expressing interneurons from both sides of the brain. Data were analysed by

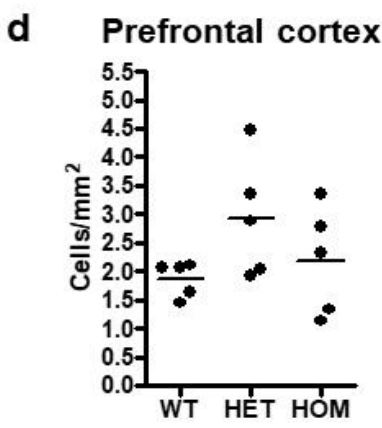
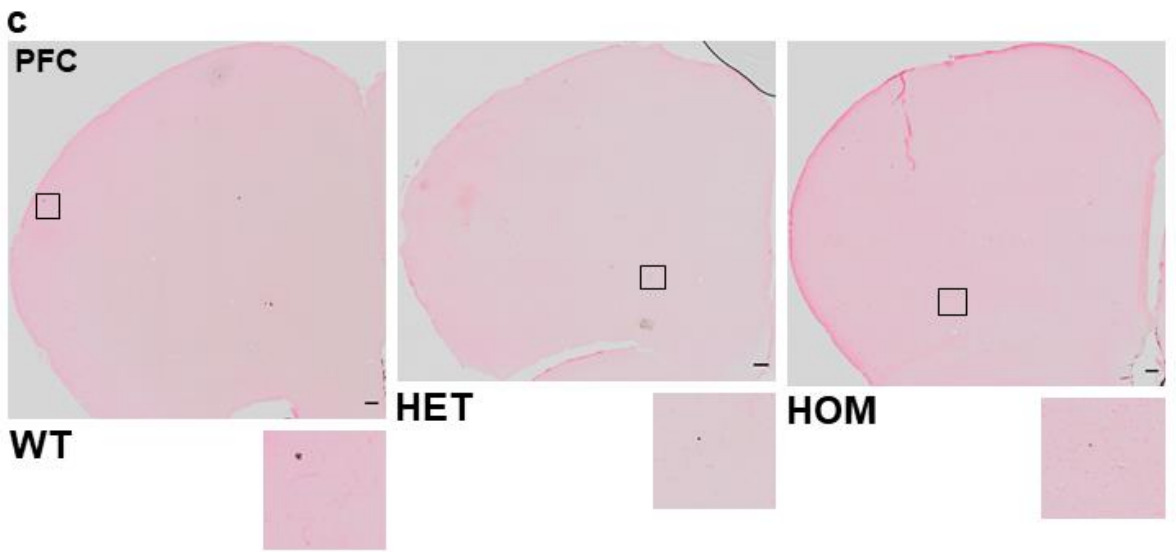
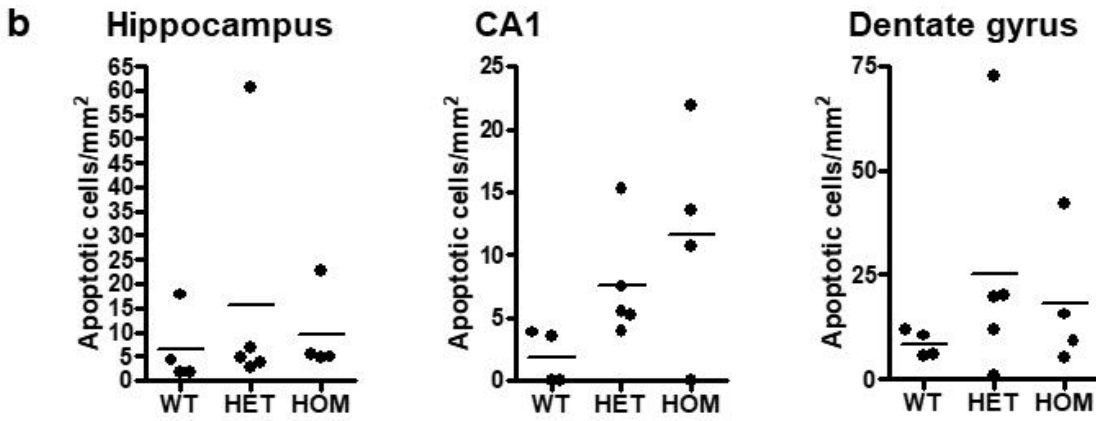
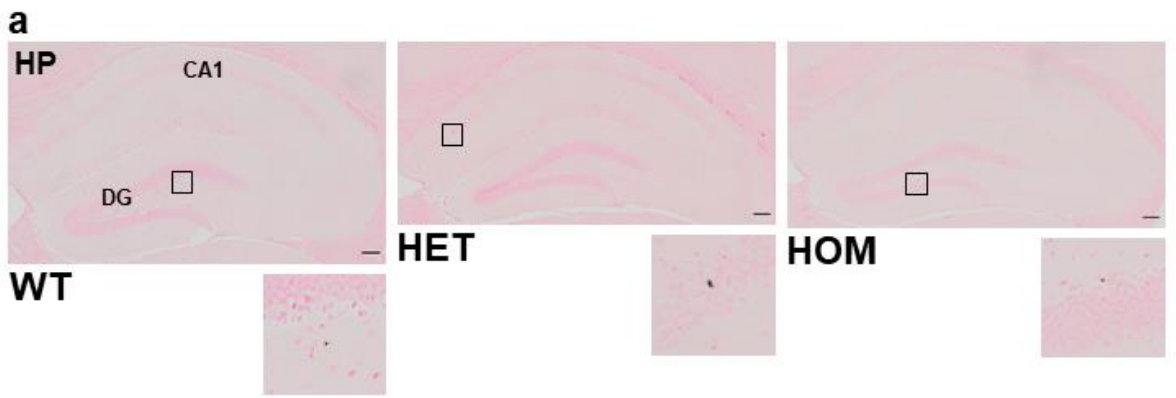
1371

Kruskal-Wallis one-way ANOVA. Horizontal line on graphs, average of values for each

1372

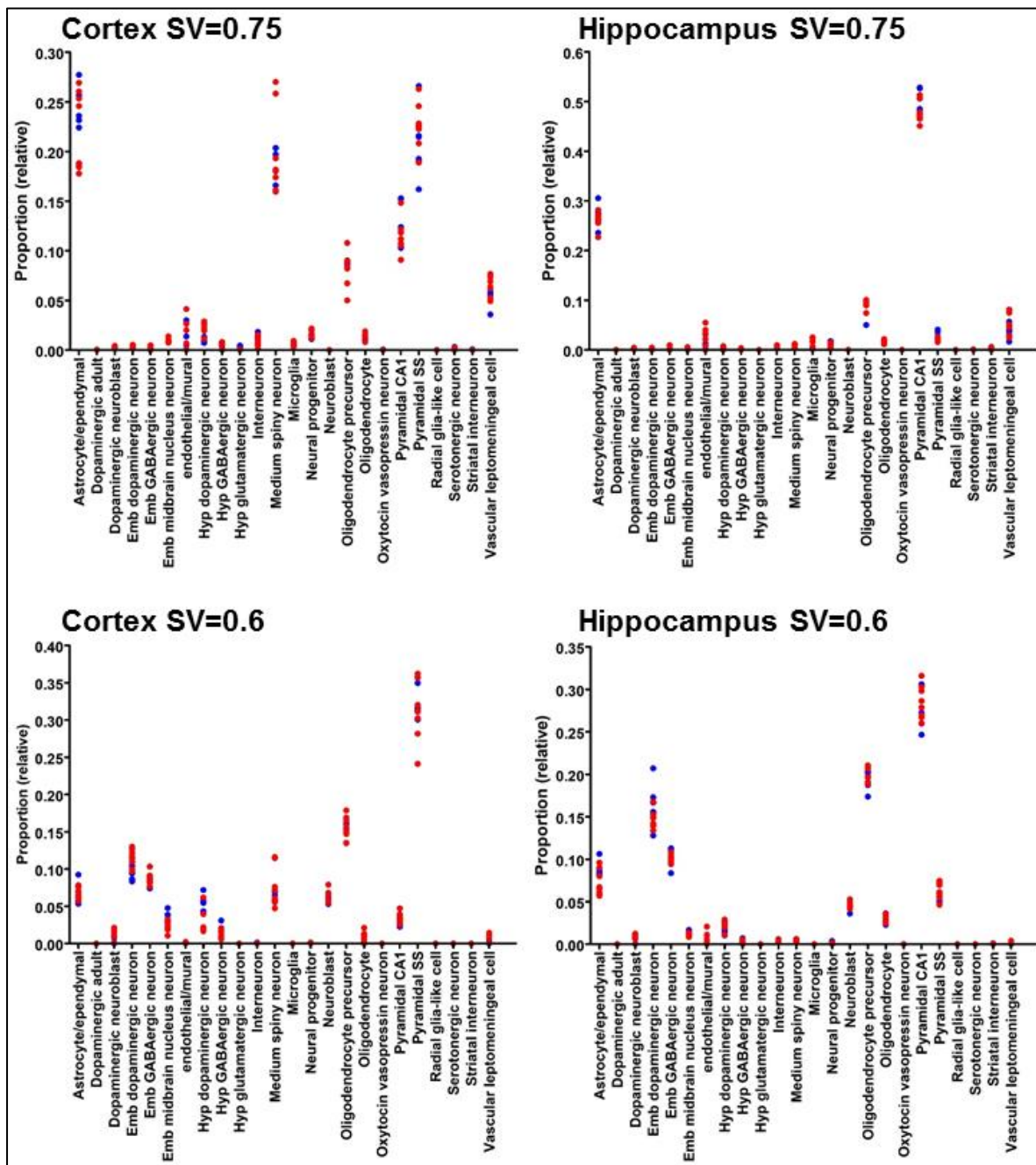
sample; WT, wild-type; HET, heterozygous *Der1*; HOM, homozygous *Der1*

1373



1375 **Supplementary Fig. 6** Quantification of apoptotic cells. **a** Hippocampal (HP) sections from
1376 nine week old mouse brain were stained with an antibody specific for Activated Caspase 3
1377 and counterstained with Nuclear Fast Red. Enlarged regions showing apoptotic cells are
1378 indicated by white boxes. **b** Average density of hippocampal apoptotic cells from both sides
1379 of the brain. Hippocampus refers to the whole hippocampal formation. **c** Prefrontal cortex
1380 (PFC) sections from nine week old mouse brain were stained with an antibody specific for
1381 Activated Caspase 3 and counterstained with Nuclear Fast Red. Enlarged regions showing
1382 apoptotic cells are indicated by boxes. **d** Average density of PFC apoptotic cells from both
1383 sides of the brain. Data were analysed by Kruskal-Wallis one-way ANOVA, $p=0.06$ for CA1.
1384 Horizontal line on graphs, average of values for each sample; WT, wild-type; HET,
1385 heterozygous *Der1*; HOM, homozygous *Der1*; DG, dentate gyrus; scale bars, 100 μ m

1387 **Supplementary Fig. 7** Test deconvolution of the 24 Superset cell classes¹⁵. Reference
1388 profiles were generated using stringent specificity value (SV) thresholds of 0.75 or 0.6 to
1389 ensure that each cell class was represented by its most specific genes. *In silico* samples
1390 were created by mixing the thresholded gene expression profiles in proportions between 0
1391 and 0.5. CIBERSORT input was compared to output and Pearson correlation coefficient and
1392 R^2 calculated to assess the quality of deconvolution of each artificial sample.
1393



1395

1396 **Supplementary Fig. 8** Deconvolution of heterozygous *Der1* cortex and hippocampus1397 RNASeq data using the Superset cell class profiles¹⁵ as reference. Reference profiles were

1398 generated using stringent specificity value (SV) thresholds of 0.75 or 0.6 to ensure that each

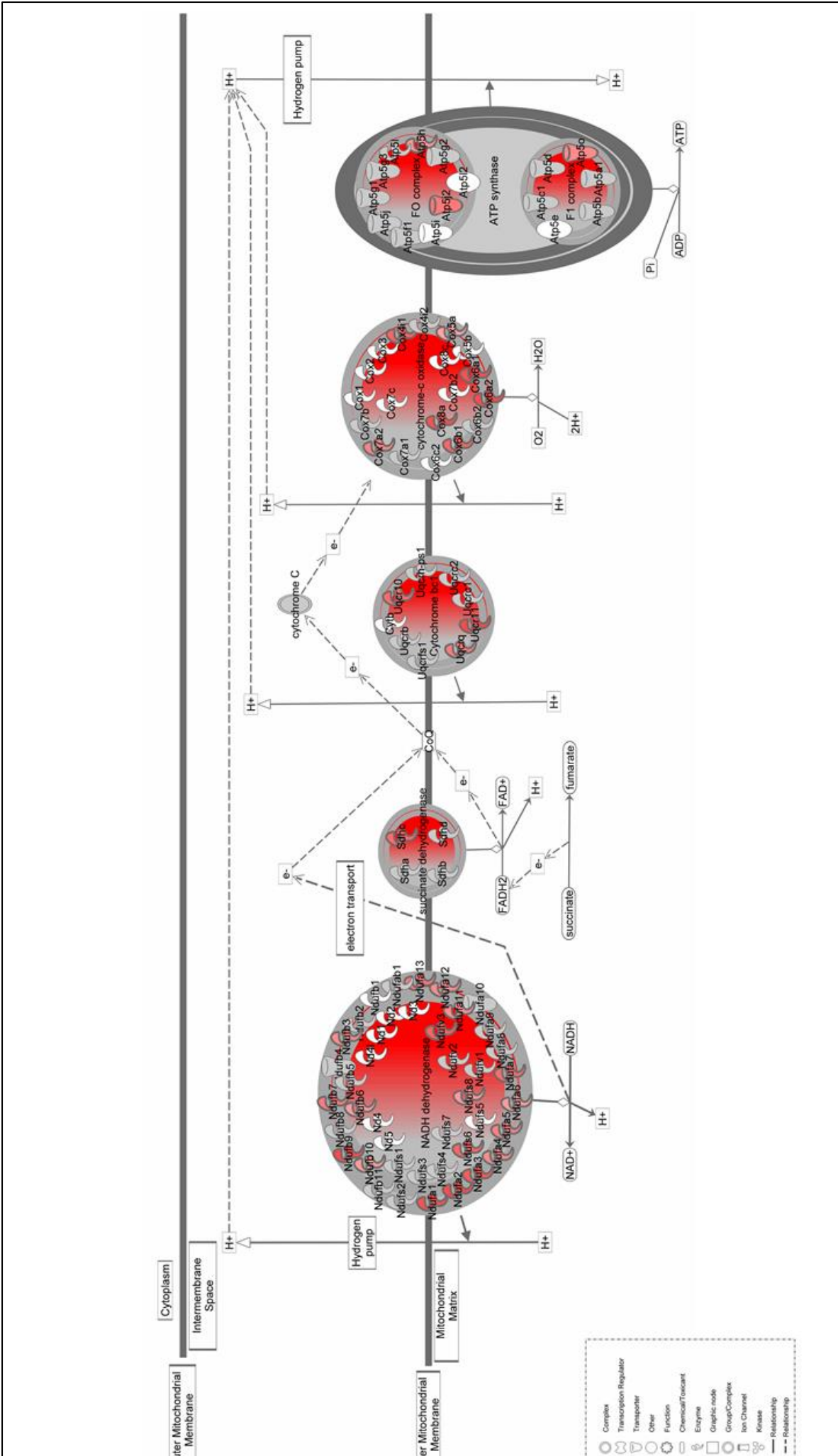
1399 cell class was represented by its most specific genes. Note that although the proportions

1400 change with the threshold set, and therefore the number of specific genes used for

1401 deconvolution, the relative proportions of each cell class do not differ between genotypes.

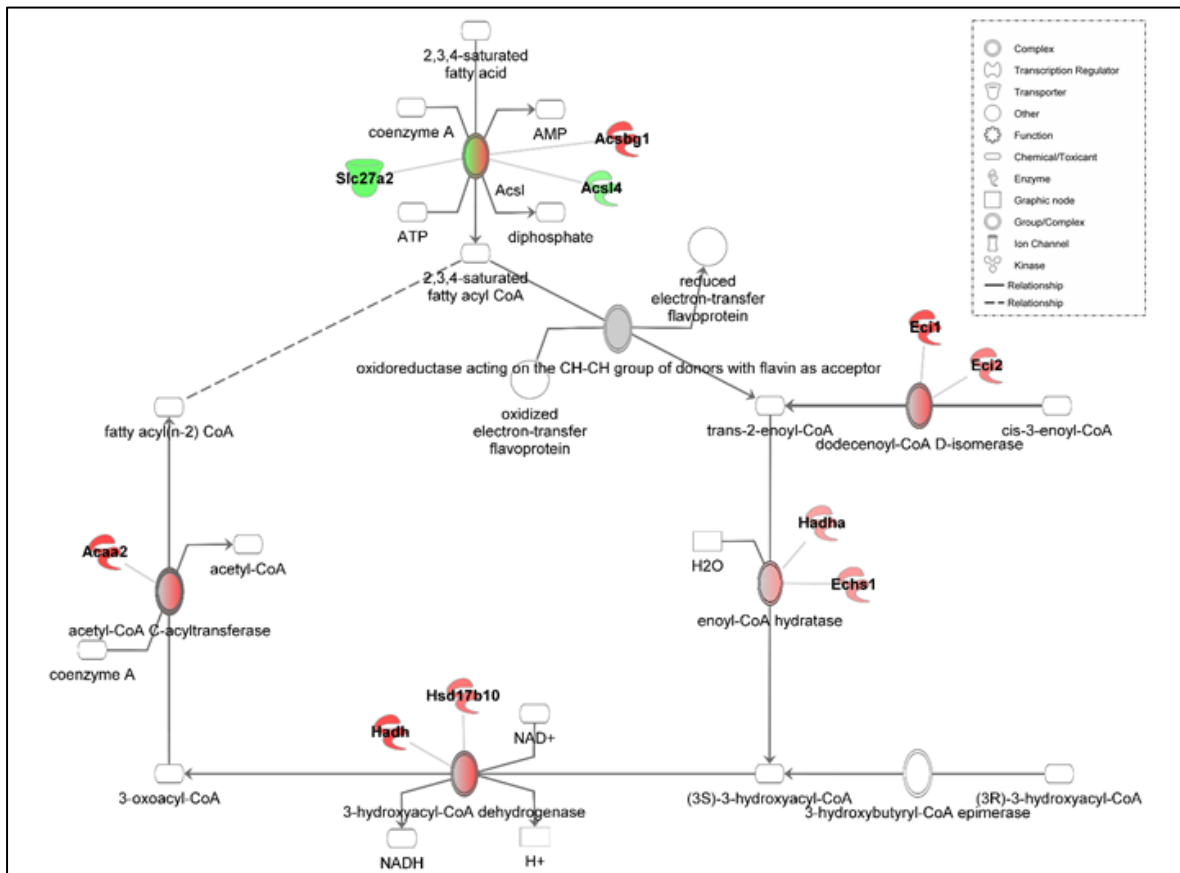
1402 Samples from embryonic cell types, neural progenitors and neuroblasts were not accurately
1403 deconvolved by CIBERSORT, thus their apparently high levels in the wild-type and *Der1*
1404 tissue are not an indication of true prevalence. Blue, wild-type; red, *Der1* heterozygote; Emb,
1405 embryonic

1406



1408 **Supplementary Fig. 9** *Der1* cortex gene dysregulation within the 'Oxidative phosphorylation'
1409 canonical pathway. Pathway impairment was predicted by IPA based on gene dysregulation
1410 at the whole gene level using DESeq2 data. Double outlines indicate protein complexes, the
1411 components of which can be found in Supplementary Table 2a, b. Colour intensity
1412 represents strength of gene expression change. green, downregulated; red, upregulated
1413

1414



1416 **Supplementary Fig. 10** *Der1* cortex gene dysregulation within the 'Fatty acid β -oxidation I'

1417 canonical pathway. Pathway impairment was predicted by IPA based on gene dysregulation

1418 at the whole gene level using DESeq2 data. Double outlines indicate enzyme complexes. To

1419 provide additional information, genes encoding relevant dysregulated enzymes and a

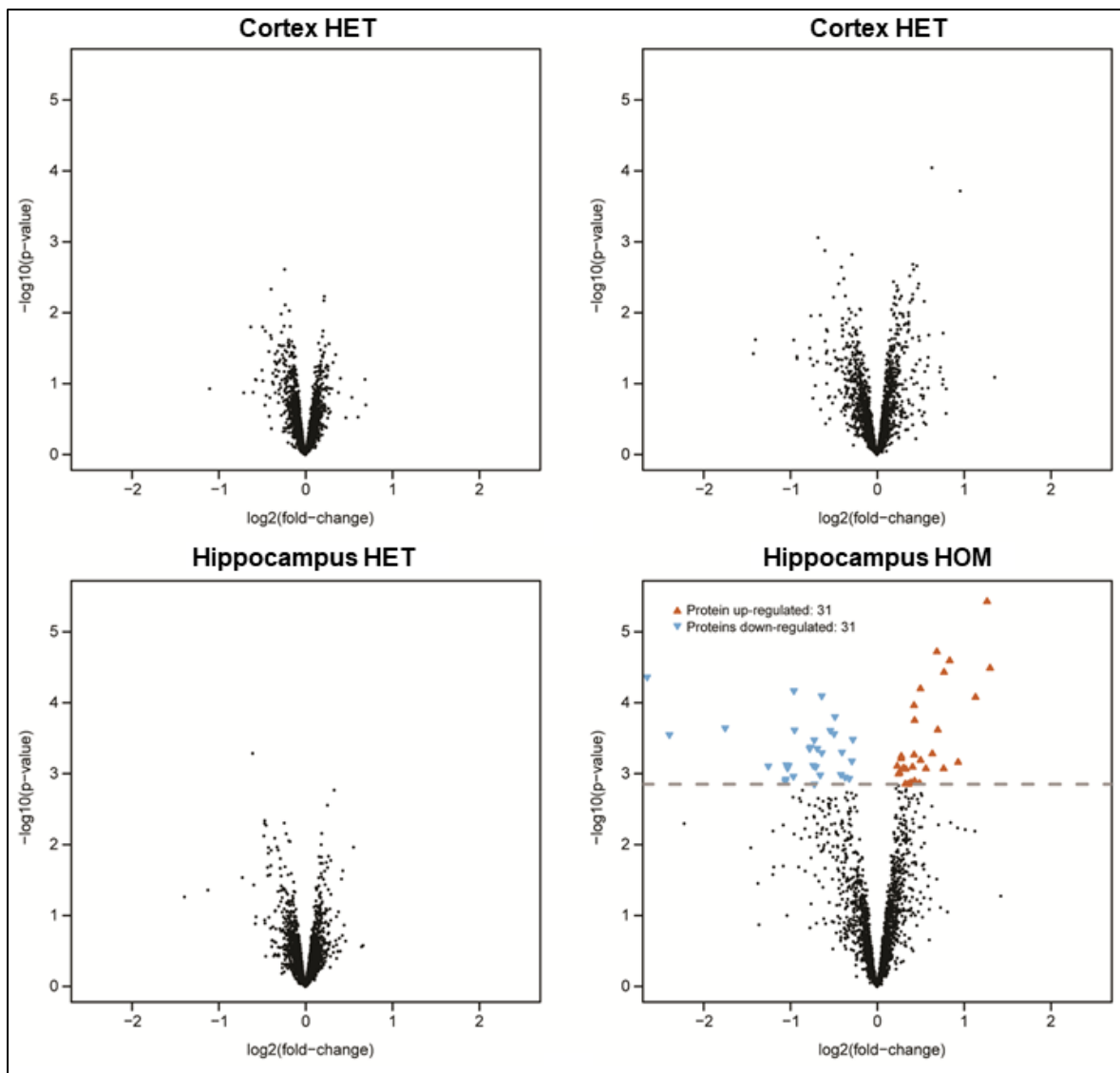
1420 transporter have been added to the pathway using the IPA 'Build' tool. Colour intensity

1421 represents strength of gene expression change, with graded colour within double outlined

1422 symbols representing overall direction of change within protein complexes. green,

1423 downregulated; red, upregulated

1424



1425

1426 **Supplementary Fig. 11** Volcano plots showing differentially expressed synaptosomes
 1427 proteins in comparisons between *Der1* mice and wild-type controls. No significant
 1428 differences were found after multiple testing correction in cortex from heterozygous and
 1429 homozygous *Der1* mice, nor in hippocampus from heterozygous *Der1* mice. In hippocampus
 1430 from homozygous *Der1* mice, 62 proteins were found to be significantly dysregulated (FDR
 1431 adjusted p-value ≤ 0.05) as indicated by the coloured dots above the dashed line.

1432

1433 **References**

- 1434 1. Malavasi ELV, Economides KD, Grunewald E, Makedonopoulou P, Gautier P, Mackie S *et al.*
1435 DISC1 regulates N-methyl-D-aspartate receptor dynamics: abnormalities induced by a Disc1
1436 mutation modelling a translocation linked to major mental illness. *Transl Psychiatry* 2018;
1437 **8(1)**: 184.
- 1438
1439 2. Jenkinson M, Beckmann CF, Behrens TE, Woolrich MW, Smith SM. *Fsl. NeuroImage* 2012;
1440 **62(2)**: 782-790.
- 1441
1442 3. Avants BB, Tustison NJ, Song G, Cook PA, Klein A, Gee JC. A reproducible evaluation of ANTs
1443 similarity metric performance in brain image registration. *NeuroImage* 2011; **54(3)**: 2033-
1444 2044.
- 1445
1446 4. Richetto J, Chesters R, Cattaneo A, Labouesse MA, Gutierrez AMC, Wood TC *et al.* Genome-
1447 Wide Transcriptional Profiling and Structural Magnetic Resonance Imaging in the Maternal
1448 Immune Activation Model of Neurodevelopmental Disorders. *Cereb Cortex* 2017; **27(6)**:
1449 3397-3413.
- 1450
1451 5. Wood TC, Simmons C, Hurley SA, Vernon AC, Torres J, Dell'Acqua F *et al.* Whole-brain ex-vivo
1452 quantitative MRI of the cuprizone mouse model. *PeerJ* 2016; **4**: e2632.
- 1453
1454 6. Tustison NJ, Avants BB, Cook PA, Zheng Y, Egan A, Yushkevich PA *et al.* N4ITK: improved N3
1455 bias correction. *IEEE Trans Med Imaging* 2010; **29(6)**: 1310-1320.
- 1456
1457 7. Dorr AE, Lerch JP, Spring S, Kabani N, Henkelman RM. High resolution three-dimensional
1458 brain atlas using an average magnetic resonance image of 40 adult C57Bl/6J mice.
1459 *NeuroImage* 2008; **42(1)**: 60-69.
- 1460
1461 8. Avants BB, Yushkevich P, Pluta J, Minkoff D, Korczykowski M, Detre J *et al.* The optimal
1462 template effect in hippocampus studies of diseased populations. *NeuroImage* 2010; **49(3)**:
1463 2457-2466.
- 1464
1465 9. Paxinos G, Franklin KBJ. The mouse brain in stereotaxic co-ordinates. 4 edn. Elsevier
1466 Academic Press: Amsterdam, The Netherlands, 2013.
- 1467
1468 10. Jiang H, Lei R, Ding SW, Zhu S. Skewer: a fast and accurate adapter trimmer for next-
1469 generation sequencing paired-end reads. *BMC Bioinformatics* 2014; **15**: 182.
- 1470
1471 11. Dobin A, Davis CA, Schlesinger F, Drenkow J, Zaleski C, Jha S *et al.* STAR: ultrafast universal
1472 RNA-seq aligner. *Bioinformatics (Oxford, England)* 2013; **29(1)**: 15-21.
- 1473
1474 12. Anders S, Pyl PT, Huber W. HTSeq--a Python framework to work with high-throughput
1475 sequencing data. *Bioinformatics (Oxford, England)* 2015; **31(2)**: 166-169.

- 1476
1477 13. Love MI, Huber W, Anders S. Moderated estimation of fold change and dispersion for RNA-
1478 seq data with DESeq2. *Genome biology* 2014; **15**(12): 550.
- 1479
1480 14. Anders S, Reyes A, Huber W. Detecting differential usage of exons from RNA-seq data.
1481 *Genome Res* 2012; **22**(10): 2008-2017.
- 1482
1483 15. Skene NG, Bryois J, Bakken TE, Breen G, Crowley JJ, Gaspar HA *et al.* Genetic identification of
1484 brain cell types underlying schizophrenia. *Nature genetics* 2018; **50**(6): 825-833.
- 1485
1486 16. Newman AM, Liu CL, Green MR, Gentles AJ, Feng W, Xu Y *et al.* Robust enumeration of cell
1487 subsets from tissue expression profiles. *Nat Methods* 2015; **12**(5): 453-457.
- 1488
1489 17. Pandya NJ, Koopmans F, Slotman JA, Paliukhovich I, Houtsmuller AB, Smit AB *et al.*
1490 Correlation profiling of brain sub-cellular proteomes reveals co-assembly of synaptic
1491 proteins and subcellular distribution. *Sci Rep* 2017; **7**(1): 12107.
- 1492
1493 18. Koopmans F, Pandya NJ, Franke SK, Phillippens I, Paliukhovich I, Li KW *et al.* Comparative
1494 Hippocampal Synaptic Proteomes of Rodents and Primates: Differences in Neuroplasticity-
1495 Related Proteins. *Front Mol Neurosci* 2018; **11**: 364.
- 1496
1497 19. He E, Lozano MAG, Stringer S, Watanabe K, Sakamoto K, den Oudsten F *et al.* MIR137
1498 schizophrenia-associated locus controls synaptic function by regulating synaptogenesis,
1499 synapse maturation and synaptic transmission. *Human molecular genetics* 2018; **27**(11):
1500 1879-1891.
- 1501
1502 20. Bruderer R, Bernhardt OM, Gandhi T, Miladinovic SM, Cheng LY, Messner S *et al.* Extending
1503 the limits of quantitative proteome profiling with data-independent acquisition and
1504 application to acetaminophen-treated three-dimensional liver microtissues. *Mol Cell*
1505 *Proteomics* 2015; **14**(5): 1400-1410.
- 1506
1507 21. Koopmans F, van Nierop P, Andres-Alonso M, Byrnes A, Cijssouw T, Coba MP *et al.* SynGO: An
1508 Evidence-Based, Expert-Curated Knowledge Base for the Synapse. *Neuron* 2019; **103**(2): 217-
1509 234 e214.
- 1510
1511 22. Martel MA, Ryan TJ, Bell KF, Fowler JH, McMahan A, Al-Mubarak B *et al.* The subtype of
1512 GluN2 C-terminal domain determines the response to excitotoxic insults. *Neuron* 2012;
1513 **74**(3): 543-556.
- 1514
1515 23. McKay S, Ryan TJ, McQueen J, Indersmitten T, Marwick KFM, Hasel P *et al.* The
1516 Developmental Shift of NMDA Receptor Composition Proceeds Independently of GluN2
1517 Subunit-Specific GluN2 C-Terminal Sequences. *Cell Rep* 2018; **25**(4): 841-851 e844.
- 1518
1519 24. Kammers K, Cole RN, Tiengwe C, Ruczinski I. Detecting Significant Changes in Protein
1520 Abundance. *EuPA Open Proteom* 2015; **7**: 11-19.

- 1521
1522 25. Smyth GK, Michaud J, Scott HS. Use of within-array replicate spots for assessing differential
1523 expression in microarray experiments. *Bioinformatics (Oxford, England)* 2005; **21**(9): 2067-
1524 2075.
- 1525
1526 26. Vasistha NA, Johnstone M, Barton SK, Mayerl SE, Thangaraj Selvaraj B, Thomson PA *et al.*
1527 Familial t(1;11) translocation is associated with disruption of white matter structural
1528 integrity and oligodendrocyte-myelin dysfunction. *Molecular psychiatry* 2019.
- 1529
1530 27. Ji B, Higa KK, Kim M, Zhou L, Young JW, Geyer MA *et al.* Inhibition of protein translation by
1531 the DISC1-Boymaw fusion gene from a Scottish family with major psychiatric disorders.
1532 *Human molecular genetics* 2014; **23**(21): 5683-5705.
- 1533
1534 28. Eykelenboom JE, Briggs GJ, Bradshaw NJ, Soares DC, Ogawa F, Christie S *et al.* A t(1;11)
1535 translocation linked to schizophrenia and affective disorders gives rise to aberrant chimeric
1536 DISC1 transcripts that encode structurally altered, deleterious mitochondrial proteins.
1537 *Human molecular genetics* 2012; **21**(15): 3374-3386.
- 1538
1539 29. Kuroda K, Yamada S, Tanaka M, Iizuka M, Yano H, Mori D *et al.* Behavioral alterations
1540 associated with targeted disruption of exons 2 and 3 of the Disc1 gene in the mouse. *Human*
1541 *molecular genetics* 2011; **20**(23): 4666-4683.
- 1542
1543 30. Umeda K, Iritani S, Fujishiro H, Sekiguchi H, Torii Y, Habuchi C *et al.* Immunohistochemical
1544 evaluation of the GABAergic neuronal system in the prefrontal cortex of a DISC1 knockout
1545 mouse model of schizophrenia. *Synapse* 2016; **70**(12): 508-518.
- 1546
1547 31. Nakai T, Nagai T, Wang R, Yamada S, Kuroda K, Kaibuchi K *et al.* Alterations of GABAergic and
1548 dopaminergic systems in mutant mice with disruption of exons 2 and 3 of the Disc1 gene.
1549 *Neurochemistry international* 2014; **74**: 74-83.
- 1550
1551 32. Iritani S, Sekiguchi H, Habuchi C, Torii Y, Kuroda K, Kaibuchi K *et al.* Catecholaminergic
1552 neuronal network dysfunction in the frontal lobe of a genetic mouse model of schizophrenia.
1553 *Acta Neuropsychiatr* 2016; **28**(2): 117-123.
- 1554
1555 33. Tsuboi D, Kuroda K, Tanaka M, Namba T, Iizuka Y, Taya S *et al.* Disrupted-in-schizophrenia 1
1556 regulates transport of ITPR1 mRNA for synaptic plasticity. *Nature neuroscience* 2015; **18**(5):
1557 698-707.
- 1558
1559 34. Tang W, Thevathasan JV, Lin Q, Lim KB, Kuroda K, Kaibuchi K *et al.* Stimulation of Synaptic
1560 Vesicle Exocytosis by the Mental Disease Gene DISC1 is Mediated by N-Type Voltage-Gated
1561 Calcium Channels. *Front Synaptic Neurosci* 2016; **8**: 15.
- 1562
1563 35. Shahani N, Seshadri S, Jaaro-Peled H, Ishizuka K, Hirota-Tsuyada Y, Wang Q *et al.* DISC1
1564 regulates trafficking and processing of APP and Abeta generation. *Molecular psychiatry*
1565 2015; **20**(7): 874-879.

- 1566
1567 36. Delevich K, Jaaro-Peled H, Penzo M, Sawa A, Li B. Parvalbumin Interneuron Dysfunction in a
1568 Thalamo-Prefrontal Cortical Circuit in Disc1 Locus Impairment Mice. *eNeuro* 2020; **7**(2).
- 1569
1570 37. Shen S, Lang B, Nakamoto C, Zhang F, Pu J, Kuan SL *et al.* Schizophrenia-related neural and
1571 behavioral phenotypes in transgenic mice expressing truncated Disc1. *J Neurosci* 2008;
1572 **28**(43): 10893-10904.
- 1573
1574 38. Dawson N, Kurihara M, Thomson DM, Winchester CL, McVie A, Hedde JR *et al.* Altered
1575 functional brain network connectivity and glutamate system function in transgenic mice
1576 expressing truncated Disrupted-in-Schizophrenia 1. *Transl Psychiatry* 2015; **5**: e569.
- 1577
1578 39. Booth CA, Brown JT, Randall AD. Neurophysiological modification of CA1 pyramidal neurons
1579 in a transgenic mouse expressing a truncated form of disrupted-in-schizophrenia 1. *Eur J*
1580 *Neurosci* 2014; **39**(7): 1074-1090.
- 1581
1582 40. Pletnikov MV, Ayhan Y, Nikolskaia O, Xu Y, Ovanesov MV, Huang H *et al.* Inducible expression
1583 of mutant human DISC1 in mice is associated with brain and behavioral abnormalities
1584 reminiscent of schizophrenia. *Molecular psychiatry* 2008; **13**(2): 173-186, 115.
- 1585
1586 41. Ayhan Y, Abazyan B, Nomura J, Kim R, Ladenheim B, Krasnova IN *et al.* Differential effects of
1587 prenatal and postnatal expressions of mutant human DISC1 on neurobehavioral phenotypes
1588 in transgenic mice: evidence for neurodevelopmental origin of major psychiatric disorders.
1589 *Molecular psychiatry* 2011; **16**(3): 293-306.
- 1590
1591 42. Katsel P, Tan W, Abazyan B, Davis KL, Ross C, Pletnikov MV *et al.* Expression of mutant
1592 human DISC1 in mice supports abnormalities in differentiation of oligodendrocytes.
1593 *Schizophr Res* 2011; **130**(1-3): 238-249.
- 1594
1595 43. Katsel P, Fam P, Tan W, Khan S, Yang C, Jouroukhin Y *et al.* Overexpression of Truncated
1596 Human DISC1 Induces Appearance of Hindbrain Oligodendroglia in the Forebrain During
1597 Development. *Schizophrenia bulletin* 2018; **44**(3): 515-524.
- 1598
1599 44. Pogorelov VM, Nomura J, Kim J, Kannan G, Ayhan Y, Yang C *et al.* Mutant DISC1 affects
1600 methamphetamine-induced sensitization and conditioned place preference: a comorbidity
1601 model. *Neuropharmacology* 2012; **62**(3): 1242-1251.
- 1602
1603 45. Abazyan B, Nomura J, Kannan G, Ishizuka K, Tamashiro KL, Nucifora F *et al.* Prenatal
1604 interaction of mutant DISC1 and immune activation produces adult psychopathology.
1605 *Biological psychiatry* 2010; **68**(12): 1172-1181.
- 1606
1607 46. Kim J, Horti AG, Mathews WB, Pogorelov V, Valentine H, Brasic JR *et al.* Quantitative Multi-
1608 modal Brain Autoradiography of Glutamatergic, Dopaminergic, Cannabinoid, and Nicotinic
1609 Receptors in Mutant Disrupted-In-Schizophrenia-1 (DISC1) Mice. *Mol Imaging Biol* 2015;
1610 **17**(3): 355-363.

- 1611
1612 47. Xia M, Zhu S, Shevelkin A, Ross CA, Pletnikov M. DISC1, astrocytes and neuronal maturation:
1613 a possible mechanistic link with implications for mental disorders. *Journal of neurochemistry*
1614 2016; **138**(4): 518-524.
- 1615
1616 48. Holley SM, Wang EA, Cepeda C, Jentsch JD, Ross CA, Pletnikov MV *et al.* Frontal cortical
1617 synaptic communication is abnormal in Disc1 genetic mouse models of schizophrenia.
1618 *Schizophr Res* 2013; **146**(1-3): 264-272.
- 1619
1620 49. Xia M, Broek JA, Jouroukhin Y, Schoenfelder J, Abazyan S, Jaaro-Peled H *et al.* Cell Type-
1621 Specific Effects of Mutant DISC1: A Proteomics Study. *Mol Neuropsychiatry* 2016; **2**(1): 28-
1622 36.
- 1623
1624 50. Hikida T, Jaaro-Peled H, Seshadri S, Oishi K, Hookway C, Kong S *et al.* Dominant-negative
1625 DISC1 transgenic mice display schizophrenia-associated phenotypes detected by measures
1626 translatable to humans. *Proceedings of the National Academy of Sciences of the United*
1627 *States of America* 2007; **104**(36): 14501-14506.
- 1628
1629 51. Altimus C, Harrold J, Jaaro-Peled H, Sawa A, Foster DJ. Disordered ripples are a common
1630 feature of genetically distinct mouse models relevant to schizophrenia. *Mol Neuropsychiatry*
1631 2015; **1**(1): 52-59.
- 1632
1633 52. Cardarelli RA, Martin R, Jaaro-Peled H, Sawa A, Powell EM, O'Donnell P. Dominant-Negative
1634 DISC1 Alters the Dopaminergic Modulation of Inhibitory Interneurons in the Mouse
1635 Prefrontal Cortex. *Mol Neuropsychiatry* 2018; **4**(1): 20-29.
- 1636
1637 53. Niwa M, Jaaro-Peled H, Tankou S, Seshadri S, Hikida T, Matsumoto Y *et al.* Adolescent stress-
1638 induced epigenetic control of dopaminergic neurons via glucocorticoids. *Science (New York,*
1639 *NY* 2013; **339**(6117): 335-339.
- 1640
1641 54. Deng D, Jian C, Lei L, Zhou Y, McSweeney C, Dong F *et al.* A prenatal interruption of DISC1
1642 function in the brain exhibits a lasting impact on adult behaviors, brain metabolism, and
1643 interneuron development. *Oncotarget* 2017; **8**(49): 84798-84817.
- 1644
1645 55. Koike H, Arguello PA, Kvajo M, Karayiorgou M, Gogos JA. Disc1 is mutated in the 129S6/SvEv
1646 strain and modulates working memory in mice. *Proceedings of the National Academy of*
1647 *Sciences of the United States of America* 2006; **103**(10): 3693-3697.
- 1648
1649 56. Kvajo M, McKellar H, Arguello PA, Drew LJ, Moore H, MacDermott AB *et al.* A mutation in
1650 mouse Disc1 that models a schizophrenia risk allele leads to specific alterations in neuronal
1651 architecture and cognition. *Proceedings of the National Academy of Sciences of the United*
1652 *States of America* 2008; **105**(19): 7076-7081.
- 1653
1654 57. Lepagnol-Bestel AM, Kvajo M, Karayiorgou M, Simonneau M, Gogos JA. A Disc1 mutation
1655 differentially affects neurites and spines in hippocampal and cortical neurons. *Molecular and*
1656 *cellular neurosciences* 2013; **54**: 84-92.

- 1657
1658 58. Kvjajo M, McKellar H, Drew LJ, Lepagnol-Bestel AM, Xiao L, Levy RJ *et al.* Altered axonal
1659 targeting and short-term plasticity in the hippocampus of Disc1 mutant mice. *Proceedings of*
1660 *the National Academy of Sciences of the United States of America* 2011; **108**(49): E1349-
1661 1358.
- 1662
1663 59. Crabtree GW, Sun Z, Kvjajo M, Broek JA, Fenelon K, McKellar H *et al.* Alteration of Neuronal
1664 Excitability and Short-Term Synaptic Plasticity in the Prefrontal Cortex of a Mouse Model of
1665 Mental Illness. *J Neurosci* 2017; **37**(15): 4158-4180.
- 1666
1667